The Stationary Wave Response to a Tropical SST Anomaly in an Idealized GCM

MINGFANG TING

Program in the Atmospheric and Oceanic Sciences, Princeton University, Princeton, New Jersey

ISAAC M. HELD

Geophysical Fluid Dynamics Laboratory/NOAA, Princeton, New Jersey

(Manuscript received 1 February 1990, in final form 16 May 1990)

ABSTRACT

The upper tropospheric stationary wave response to a tropical sea surface temperature (SST) anomaly is examined with an idealized general circulation model (GCM) as well as steady linear and nonlinear models. The control climate of the GCM is zonally symmetric; this symmetric climate is then perturbed by a dipolar SST anomaly centered at the equator. Two experiments, with anomaly amplitudes differing by a fact of two, have been conducted. The response is very linear in the amplitude of the SST anomaly.

A steady, baroclinic model linearized about a zonally symmetric basic state simulates the GCM's stationary wave reasonably well when it is forced by anomalous heating as well as anomalous transients. When decomposing the GCMs flow into parts forced separately by heating and transients, tropical transients are found to play a dissipative role to first approximation, reducing the amplitude of the response to heating by a factor of two. The effects of extratropical transients are relatively weak. A steady nonlinear model is also used to evaluate the importance of transients and confirms the diagnosis based on the linear model.

Part of the tropical transients seems to be forced by tropical convection and part by midlatitude disturbances propagating into the tropics. The anomalous extratropical transients include a part related to a shift in the model's storm track and a part related to barotropic instability of the stationary wave, but the effects of both of these changes are relatively weak due to the absence of strong extratropical climatic zonal asymmetries in the model.

The dissipative role of transients in this model is contrasted with the positive feedback found by Held et al. (1989) in a GCM with realistic boundary conditions. The calculations in that paper are repeated, and the direct linear response to thermal forcing is found to be sensitive to the damping included in the model; but the positive feedback from the transients is robust to changes in the linear model. We speculate that a strong asymmetric storm track, with a well-defined barotropic decay region, is needed for the positive feedback to occur.

1. Introduction

The atmosphere's climatic response to tropical sea surface temperature (SST) anomalies remains a challenging problem in general circulation research. This response is of great importance for interannual variability in both tropical and extratropical regions. Atmospheric general circulation models (GCMs) have been widely used to study both the anomalous tropical heating field induced by an SST anomaly and the circulation anomalies forced by this heating field. In addition, a variety of linear modeling studies have examined the response of the circulation to a given heating anomaly. These range from models of the tropical response that are simply linearized about a state of rest, to models of the extratropical response linearized about a zonally symmetric basic state, to models linearized about the observed zonally asymmetric climate. Studies of the ways in which nonlinearity modifies the steady response to tropical heating have also begun (e.g., Sardeshmukh and Hoskins 1985; Hendon 1986; Haarsma and Opsteegh 1989). In the present study, we use an idealized GCM to predict the atmospheric response to a tropical SST anomaly. This model's response is then analyzed with linear and nonlinear stationary baroclinic models. In its simultaneous use of a GCM and steady state baroclinic models, this work is similar to that on the climatological wintertime stationary waves by Nigam et al. (1986, 1988), the ice age stationary waves by Cook and Held (1988), and the response to El Niño SSTs by Held et al. (1989). We believe that this combination of tools is particularly powerful in the study of the atmosphere's response to lower boundary perturbations.

The design of the GCM experiments described here is motivated by previous work with both GCMs and with linear models that emphasizes the importance of the interaction of a wavetrain emanating from anomalous heating in the tropics with the climatological sta-

Corresponding author address: Dr. Mingfang Ting, CIRES, University of Colorado, Campus Box 216, Boulder, CO 80309-0216.

tionary waves and/or transients in midlatitudes. Among the GCM experiments, one that raises this issue particularly clearly is that of Geisler et al. (1983). Using the NCAR Community Climate Model (CCM), they test the sensitivity of the Northern Hemisphere wintertime circulation to the location and size of a tropical warm anomaly. They find that while the tropical response shifts as the SST anomaly moves in longitude, the extratropical response is relatively insensitive to the position of the anomaly, always showing a structure that can be loosely termed the Pacific/North American (PNA) pattern. Further evidence that wavetrains interact with longitudinal asymmetries in the climate has been found by Palmer and Mansfield (1986) and Blackmon et al. (1987), who found that the extratropical response to tropical SST anomaly depends on the amplitude of the climatological asymmetries in midlatitudes.

Linear modeling studies have pointed in the same direction. Using a barotropic model, Simmons (1982) modified the simple picture presented by Hoskins and Karoly (1981) of Rossby waves emanating from a tropical source by demonstrating that the extratropical response to tropical heating can be enhanced by linearizing about the observed zonally asymmetric flow rather than about a zonally symmetric flow. Simmons et al. (1983) help to explain this stronger response by noting that the wintertime climatological upper tropospheric flow is barotropically unstable, with one phase of an unstable mode resembling the PNA pattern. (See also Branstator 1985.) Trenberth et al. (1988) have recently argued that the anomalous circulation over North America during the *summer* of 1988 was the response to the northward movement of the ITCZ in the eastern Pacific resulting from strong anti-El Niño conditions. Once again, linearizing about a zonally asymmetric rather than a symmetric basic state is central to their result.

A different picture is painted by Held et al. (1989) (hereafter HLN), who analyze the composited El Niño and anti-El Niño events simulated by a GFDL GCM. In this GCM, the ocean temperatures are fixed at their climatological values everywhere except in the tropical Pacific, where the observed SSTs during the 1962–76 period are imposed (Lau 1985). HLN use a baroclinic model linearized about a zonally symmetric basic state to simulate the difference between the El Niño and anti-El Niño composites. When forced with the anomalous heating and the anomalous fluxes due to transients in the GCM composites, this linear model provides a reasonably accurate simulation of the flow anomalies. When this response is decomposed into parts forced separately by the heating anomaly and the anomaly in the transient fluxes, the response to the anomalous transients is found to dominate. The direct response to tropical heating is small, although of the correct phase in the Pacific sector. The dominance of the forcing by transient eddy fluxes is consistent with the analysis by Kok and Opsteegh (1985) of the observed extratropical response to the 1982–83 ENSO event. Anomalies in both the tropical and extratropical transient eddy fluxes are found to be important by HLN. In northern midlatitudes, there is a shift in storm track position in the eastern Pacific that feeds back strongly on the tropically forced wavetrain. (As discussed in section 6, in repeating the calculations of HLN with the model described here, we find that the direct response to tropical heating is sensitive to the imposed dissipation used by HLN, and its amplitude can be made comparable to the GCM response if this dissipation is made sufficiently weak. However, the conclusion that there is strong positive feedback from the transients remains valid.)

The results in HLN need not be inconsistent with the GCM calculations described previously. First, the importance of the interaction between the anomalous and the climatological stationary waves can be sensitive to the details of the forcing. The barotropic calculations in Held and Kang (1987) indicate that this interaction would be much larger in the GCM than in the HLN study if the heating anomaly in the western Pacific north of the equator were larger. Second, the influence of the climatological stationary eddies on the response can occur through storm track structure as well as through direct interaction of the mean fields. It may be that a strongly asymmetric storm track, with a well-defined barotropic decay region, responds much more strongly to a modest signal from the tropics than does a more zonally symmetric storm track. The implication would then be that the anomalous transient eddy fluxes seen in HLN would occur only when large climatological stationary waves are present to create a strongly asymmetric storm track.

Motivated by these considerations we design a GCM experiment in which a control with *zonally symmetric climate* is perturbed by a tropical SST anomaly. This kind of experiment is of interest for several reasons. Given the apparent complexity of previous GCM results, an understanding of how a zonally symmetric climate is perturbed by an SST anomaly seems to be a necessary stepping stone towards an understanding of the response in more realistic models. One expects the nonlinearity of the mean extratropical flow to be less important in such a model, so that it should be easier to diagnose the response with a model linearized about a zonally symmetric flow and determine what role anomalous transient eddy fluxes play. We are especially concerned with whether the response of an initially zonally symmetric storm track to a wavetrain emanating from the tropics is similar to or fundamentally different from the response of the strongly asymmetric Pacific storm track evident, for example, in HLN.

Such an idealized GCM experiment can also be used to study the dynamics of the tropical response. From Neelin's (1988) experience, we expect Gill's simple model, Sverdrup balance plus damping, to provide a useful fit to the GCM's response to the anomalous

heating near the surface, where the friction in the boundary layer provides the damping, but in the upper troposphere not only is advection by the mean flow significant but one also expects nonlinearity to come into play. The effects of upper tropospheric transients on the mean tropical response, generally ignored, may also play a role in the GCM. We utilize both linear and steady nonlinear models to diagnose the GCM's tropical circulation. We do not address the problem of relating the heating distribution to the SST anomaly itself.

The design of the GCM experiments and some of the characteristics of the GCM's time-mean response are given in sections 2 and 3. Section 4 contains a detailed discussion of the linear and steady nonlinear model simulations and the maintenance of both tropical and extratropical stationary waves. In section 5, the effects of the SST anomaly on the GCM's transients are discussed in more detail. In section 6 we briefly address the differences between these results and those of HLN. The Appendix contains details of the linear and nonlinear steady state models.

2. Design of GCM experiments

A σ-coordinate global spectral model constructed at GFDL with rhomboidal truncation at wavenumber 15 has been used to perform these experiments. Many of the details of the model can be found in Manabe et al. (1979) and Gordon and Stern (1982). The lower boundary is simplified to be an all-ocean surface with prescribed temperatures. For simplicity, we also remove sea ice and fix the ocean surface albedo at 0.1. The cloud distribution is also fixed and is zonally symmetric. We use perpetual January insolation at the top of the model.

Because of the perpetual January conditions and the absence of any large planetary waves in the extratropical stratosphere of this model, an extremely strong polar-night jet is formed in the top layer ($\sigma = 0.025$) in the winter hemisphere. The presence of this jet limits the size of the time step in the numerical integration. Since we confine our attention to the model's troposphere in this paper, and since the dynamics of the model's top layer is strongly affected by the rigid lid condition in any case, we add a Rayleigh friction to the top layer with a 20 day damping time to limit the size of this jet. Without producing any noticeable distortion at lower levels, this allows the use of a substantially larger time step.

We run three cases with the same model but different sea surface temperature distributions. The control run has a zonally symmetric SST distribution of the form

$$T_s(\theta) = T_0 - T_1 \sin\theta - \frac{2}{3} T_2 P_2(\sin\theta) \qquad (1)$$

where $P_2(x) = \frac{1}{2}(3x^2 - 1)$, with $T_0 = 287$ K, $T_1 = 10$ K, and $T_2 = 40$ K. The maximum temperature of nearly 301 K occurs at about 7°S. The temperature is about 270 K at the south pole and 250 K at the north pole. A second experiment has an east–west dipolar anomaly added along the equator to the zonally symmetric SST of the control run. The form of the anomaly is

$$T_A(\lambda, \theta) = A e^{-(\theta/L_y)^2}[e^{-[(\lambda-\lambda_1)/L_x]^2} - e^{-[(\lambda-\lambda_2)/L_x]^2}]. \qquad (2)$$

The longitudinal and latitudinal scales L_x and L_y are respectively 30° and 15°, and the amplitude A is 2.5 K. The separation between the two centers, $\lambda_2 - \lambda_1$, is 90°. The spatial structure, with the positive center to the west of the negative center, was chosen to roughly correspond to the temperature distribution in the equatorial Pacific. (In the plots to follow, we arbitrarily set $\lambda_1 = 150$°E, and $\lambda_2 = 120$°W, once again, with the Pacific in mind.) In the third experiment, the size of the anomaly is doubled ($A = 5$ K). These two experiments are referred to as the "weak" and "strong" anomaly runs, respectively. As described below, the two anomaly runs produce stationary eddies with very similar structures and dynamical balances. Figures 1a,b give the distribution of the anomaly and the total SST

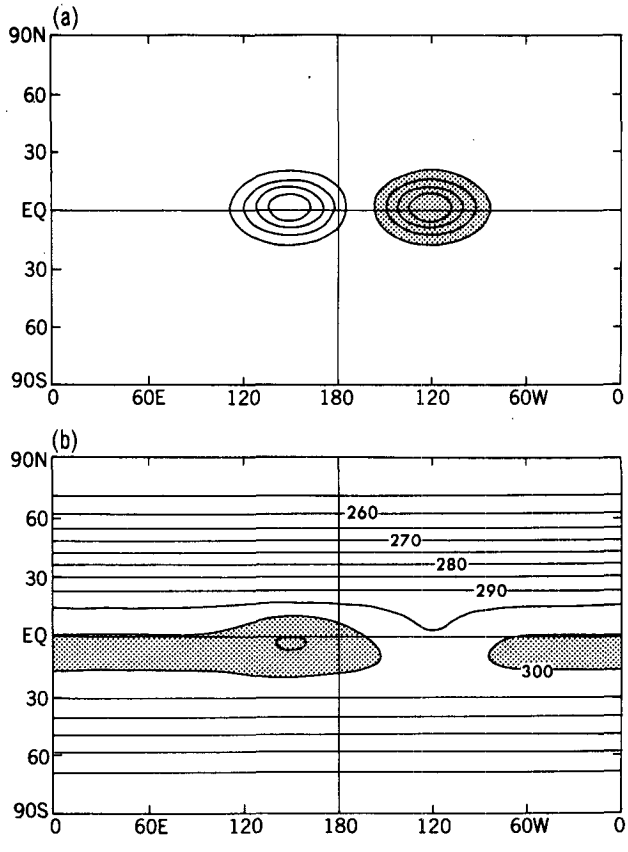

FIG. 1. The dipolar SST anomaly (a) and total SST distribution (b) in the strong anomaly case. Contour intervals are 1 K in (a) and 5 K in (b). Negative values in (a) and values greater than 300 K in (b) are shaded.

in the strong anomaly run. The maximum SST has the unrealistically high value of 306 K in this case. All three experiments have exactly the same zonally averaged SSTs.

3. GCM responses

We integrate the control experiment for 800 days after discarding an initial spin up period. The time-mean circulation from this experiment is broadly similar to the observed solstitial circulation in the troposphere. Some features of present interest are described in Fig. 2. The zonal mean precipitation (Fig. 2a) shows a sharp maximum at about 7°S, which is also the latitude of the zonally symmetric SST maximum. The meridional circulation (Fig. 2b) is very asymmetric about the equator, with the wintertime cell an order of magnitude stronger than its counterpart in the summer hemisphere. The climatological jet (Fig. 2c) has maximum westerly wind speed of 45 m s^{-1} in the Northern Hemisphere, but only 22 m s^{-1} in the Southern Hemisphere. The weak upper tropospheric westerlies at the equator are a common feature in low resolution GCMs.

The mean circulation in the anomaly experiments is obtained by averaging over 2000 days in each case. Although the zonally averaged SSTs are unchanged, these experiments do show significant changes in the zonally averaged flow. The difference between the zonally averaged zonal flows in the anomaly and control

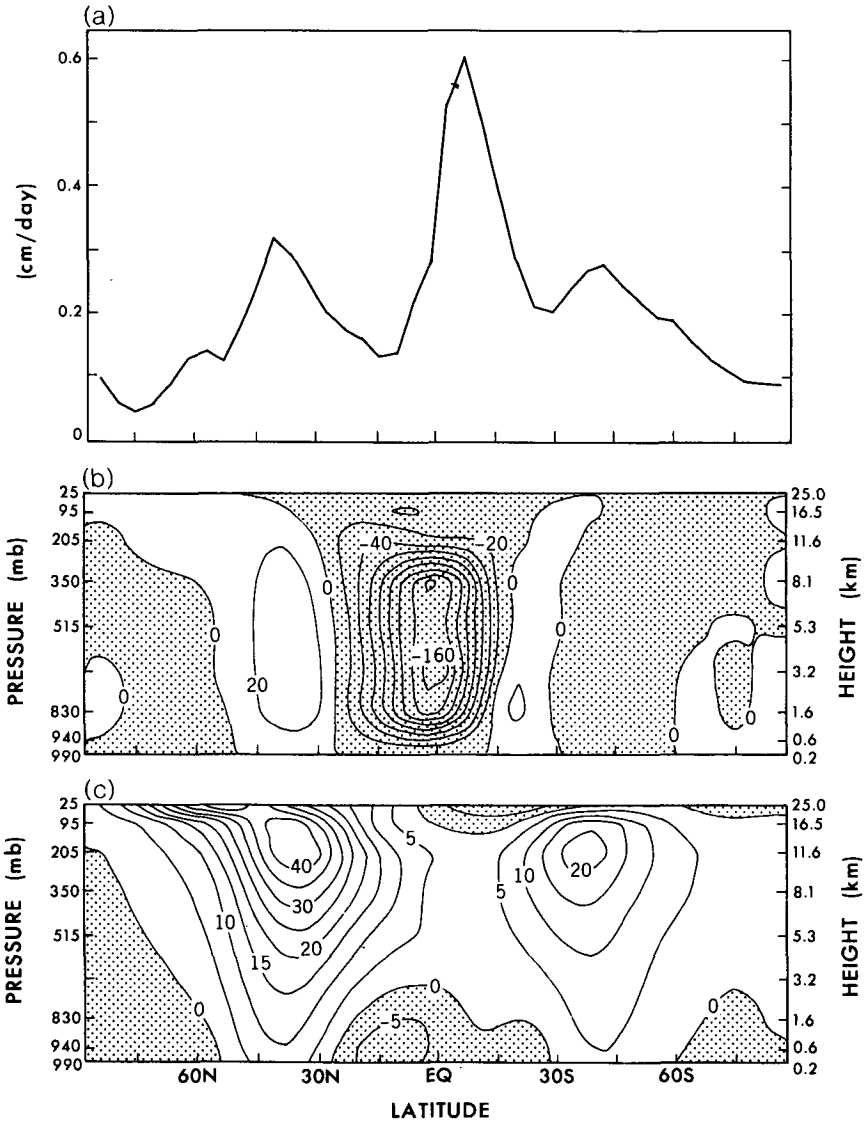

FIG. 2. Latitudinal distribution of zonal mean precipitation (a), streamfunction of meridional circulation (b), and zonal mean zonal wind (c) for control run. The contour intervals are 20 m mb s^{-1} in (b) and 5 m s^{-1} in (c). Negative values are shaded.

runs is shown in Figs. 3a,b. There is a 5 m s^{-1} increase in the westerlies at 205 mb on the equator in the strong anomaly run. The weak SST anomaly run shows a similar but weaker modification with a maximum of nearly 2 m s^{-1}. This is the qualitative response expected from wave-mean flow interaction theory for a Rossby wave excited in low latitudes: if the wave propagates poleward and is *absorbed* at higher latitudes, then the horizontal stationary eddy momentum flux should act to decelerate the flow where the wave is absorbed and accelerate it near the tropical source (e.g., Edmon et al. 1980). However, a preliminary examination of the stationary and transient eddy forcing of the mean flow suggests that the dynamics are not straightforward. In fact, the vertical stationary eddy momentum flux seems to play a more important role than the horizontal fluxes. We do not attempt to develop a simple quantitative explanation for this zonal mean response here. As described in section 4, the change in the zonal mean has only a small effect on planetary wave propagation.

Figures 4a,b show the zonally asymmetric part of the mean precipitation in the weak and strong anomaly experiments. Figure 4c shows the total precipitation pattern for the strong anomaly. (Note that the contour interval in Fig. 4a is half of that in 4b, and furthermore, in each panel, the interval north of 10°N is one-fourth of that south of this latitude, in order to highlight the extratropical signal.) Both cases show a positive (negative) rainfall anomaly centered over the center of the warm (cold) SST anomaly. The maxima in the rainfall anomalies lie south of the equator, near the latitude of the precipitation maximum in the control run, with the positive anomaly extending southeastwards and, to a much weaker extent, northeastward from the warm water. The maximum negative rainfall anomalies are 0.4 cm day^{-1} and 0.3 cm day^{-1} for the large and small anomaly cases, respectively. This lack of linearity over the cold water is not surprising. As is clear in Fig. 4c, in the large anomaly case there is little rainfall left over the cold water since the precipitation in the ITCZ of the control run is 0.6 cm day^{-1}. The response over the warm water is surprisingly linear. The maximum rainfall increase is 1.1 cm day^{-1} in Fig. 4b and 0.5 cm day^{-1} in Fig. 4a. The weak maxima at 30°N in Figs. 4a,b is due to a southward shift and intensification of the storm track. While these extratropical rainfall anomalies are much weaker than those in the tropics (~0.15 cm day^{-1} in the strong anomaly case), they are comparable to the climatological precipitation at that latitude.

The GCM's stationary wave responses to the tropical SST anomaly are displayed in Fig. 5. The 205 mb eddy zonal wind and geopotential height are shown for both the weak and strong anomaly experiments. (The contour intervals in Figs. 5a,b are once again half of those in Figs. 5c,d). Figures 5a,c show strong equatorial easterly and westerly anomalies that are centered very close to the longitudes of the warm and cold SST anomalies, respectively. The tropical part of the response is quite symmetric about the equator, much more so than the heating anomaly itself. The most noticeable asymmetry is the slight displacement of the center of the westerly

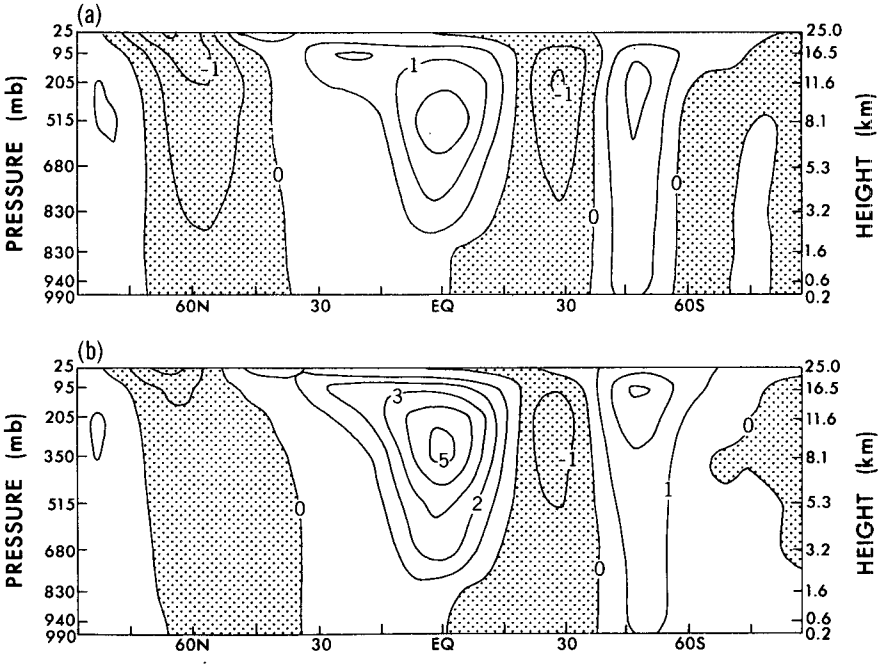

FIG. 3. The difference in zonal mean zonal wind between anomaly run and control run in weak (a) and strong (b) anomaly experiments. Contour intervals are 0.5 m s^{-1} in (a) and 1 m s^{-1} in (b). Negative values are shaded.

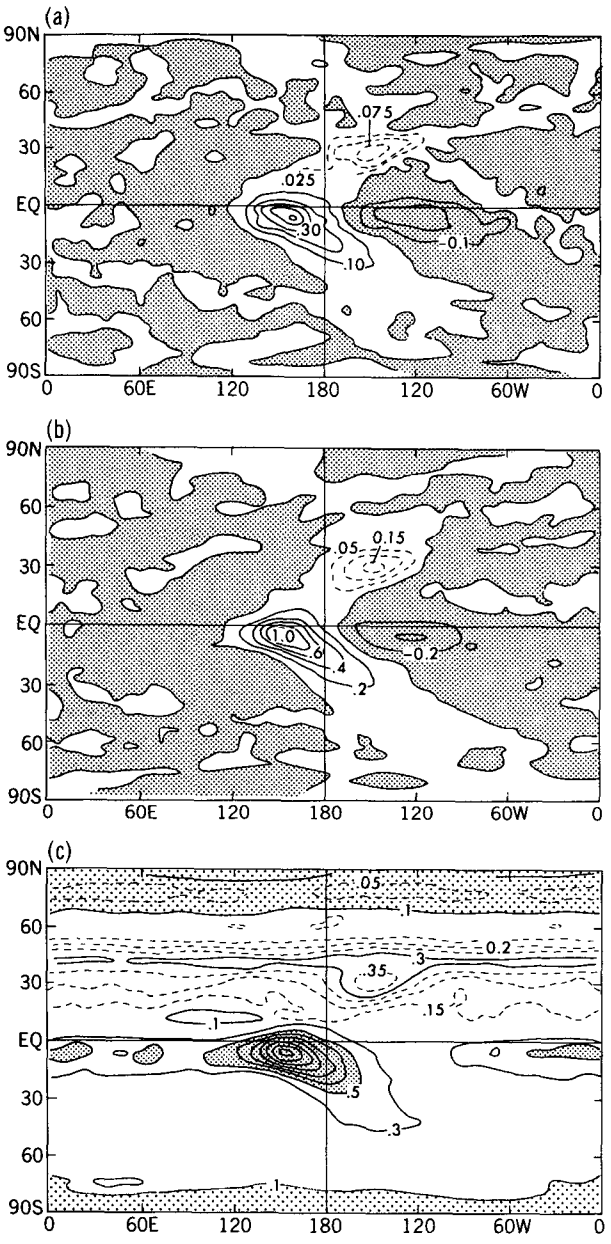

FIG. 4. Zonally asymmetric rainfall in weak (a) and strong (b) anomaly experiments. The total precipitation for the strong anomaly case is shown in (c). The contour intervals are 0.1 cm day^{-1} in (a), 0.2 cm day^{-1} in (b) and (c) south of 10°N, and 0.025 cm day^{-1} in (a) and 0.05 cm day^{-1} in (b) and (c) north of 10°N. Negative values are shaded.

wind anomaly south of the equator. There are subtropical zonal wind anomalies of opposite sign, of at most half the strength of the equatorial anomalies. For comparison, in the 1982–83 El Niño the observed subtropical zonal wind anomaly was as large as the equatorial anomaly in the Pacific (e.g., Kok and Opsteegh 1985). This is also the case in the El Niño/anti-El Niño composite of the response to observed SST anomalies in essentially the same GCM, but with realistic boundary conditions (Lau 1985). The weak subtropical wind anomalies in this idealized GCM suggest that there are interactions that are absent in this idealized model but present in more realistic models, that enhance the midlatitude signal, as one might expect from the results surveyed in the Introduction.

The geopotential heights in Figs. 5b,d further emphasize the fact that the anticyclone (cyclone) pair associated with tropical heating (cooling) is closely aligned in longitude with the forcing. This is also observed to be the case in the 1982–83 ENSO event (Hendon 1986), for example. In the simplest linear model of the response to localized heating (Gill 1980), the anticyclones are centered to the west of the heating, as expected from Sverdrup balance. It is interesting to ask if a more complete linear model can simulate the GCM's alignment or if nonlinearity is important in this regard. Hendon (1986) has pointed out that nonlinearity can shift the tropical centers eastward. It is also interesting to ask if nonlinearity is essential for capturing the symmetry of the tropical response, given the very asymmetric heating anomaly (Figs. 4a,b).

The symmetry of the response breaks down in midlatitudes, as the anomalous high at 50°N is much stronger than its Southern Hemisphere counterpart. The strength of this feature is approximately 55 gpm in the weak anomaly case and 90 gpm in the strong case. The pattern is remarkably similar in the two cases, with amplitude closely proportional to the amplitude of the SST anomaly. The most noticeable difference is an eastward displacement of the entire pattern in the strong anomaly run. This small phase shift is evident in the tropical winds and the Northern Hemisphere wavetrain.

4. Linear and nonlinear steady state models

a. Model descriptions

In order to diagnose the dynamics underlying these GCM responses, we linearize the GCM equations about a zonally symmetric state and solve the resulting equations by direct matrix inversion. The model differs from that used by Nigam et al. (1986, 1988) and HLN in that it is fully spectral in the horizontal. The resulting model is an exact linearization of the spectral GCM. The numerical method is similar to that of Schneider (1989). A brief description of the basic equations and numerical scheme is provided in the Appendix.

It is also useful to compare the GCM stationary eddies to the steady, fully nonlinear response to imposed heating. Our procedure for obtaining such a solution requires a linear model in which the basic state is fully three-dimensional—that is, zonally asymmetric. This model is also an exact linearization of the GCM equations, but because of computational requirements we do not solve it at the resolution of the GCM. Based on trial and error, we compromise on zonal, rather than

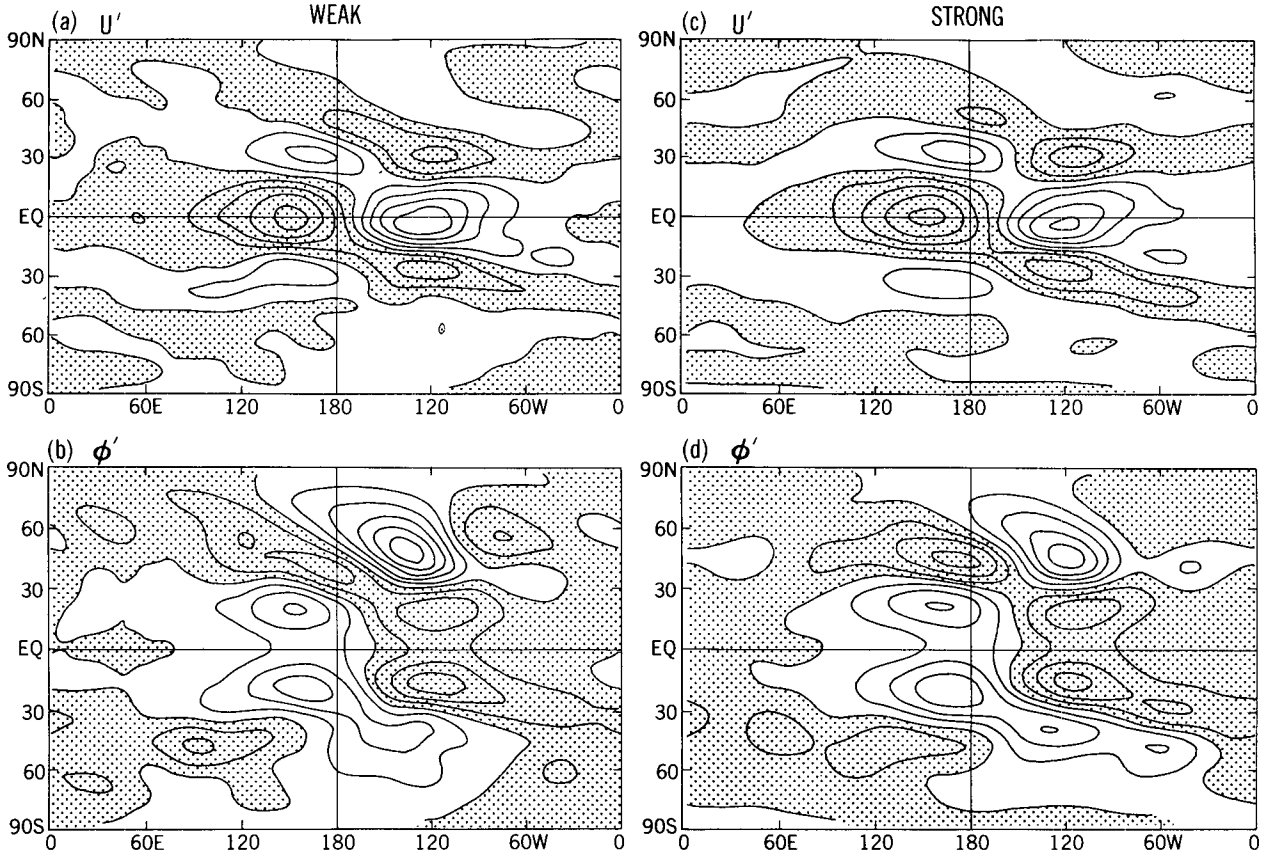

FIG. 5. Eddy zonal wind (a) and geopotential (b) in weak anomaly GCM, and eddy zonal wind (c) and geopotential (d) in strong anomaly GCM at 205 mb. Contour intervals are 2 m s^{-1} in (a), 10 gpm in (b), 4 m s^{-1} in (c) and 20 gpm in (d). Negative values are shaded.

vertical or meridional, resolution. The model is truncated to five zonal wavenumbers, but the GCMs full vertical and meridional resolution is retained. Based on a suggestion by P. Valdes, a simple iteration procedure is used to obtain fully nonlinear solutions. The zonal mean atmospheric state is prescribed; only the asymmetric part of the flow is determined by the nonlinear model. Description of the nonlinear model can also be found in the Appendix.

For simplicity, the boundary layer stresses in the GCM are parameterized as Rayleigh friction. We utilize the same scheme as that in Nigam et al. (1986), in which the damping rate is

$$\kappa = (\sigma - 0.8)/0.2, \quad \sigma > 0.8, \qquad (3)$$

in units of $(\text{day})^{-1}$. At the ground ($\sigma = 1$) the damping rate is $(1\ \text{day})^{-1}$, and falls to zero at $\sigma = 0.8$. We find it convenient to treat sensible heating in a parallel fashion; temperatures are damped back to the surface temperature at this same rate. When we specify the GCM's heating for the linear or nonlinear model, only the latent heating is included. If we do not include this thermal damping near the ground and instead include the sensible heating as a forcing, the upper tropospheric response in these models is nearly unchanged; the only effects are near the surface. Biharmonic diffusion has been included in the vorticity, divergence and temperature equations as in the GCM, but with a larger coefficient of 1×10^{17} m^4 s^{-1} (the GCM's value is 1×10^{16} m^4 s^{-1}). The larger coefficient provides a smoother response, which is useful when iterating to find nonlinear solutions.

In Nigam et al. (1986), additional mechanical damping in the tropics was found to be necessary to obtain realistic equatorial winds for the response to the climatological tropical heating field. In the present paper we do not include such a term; we wish to avoid the inclusion of damping that is meant to mimic the effect of transients and/or nonlinearity since the intention is to obtain fully nonlinear solutions and to evaluate the role of transients by imposing the transient eddy fluxes predicted by the GCM as explicit forcing. We do not encounter the difficulties found by Nigam et al. without this extra damping in the tropics. The larger biharmonic diffusion does not seem to be of particular importance in this regard; if we return to the GCM's smaller value, the equatorial zonal winds do not change substantially. The implication is that a re-

alistic upper tropospheric flow is more nonlinear than that produced by this idealized GCM.

b. *Basic state and forcing functions*

The zonally symmetric basic state ($\bar{U}$, $\bar{V}(\bar{\zeta}, \bar{D})$, $\bar{T}$, $\bar{\sigma}$, and $\overline{\ln P_*}$) in Eqs. (A1)–(A6) is taken to be the zonal mean of the GCM's time-mean flow. Unless otherwise stated, the steady linear or nonlinear models of the weak (strong) anomaly stationary waves described below, use the zonal mean flow from the weak (strong) anomaly GCM. The modest differences in the stationary wave patterns that result from using, instead, the zonal mean of the control symmetric climate, are briefly described in section 4e.

The forcing function for both linear and steady nonlinear models includes diabatic heating and the tendencies, in the vorticity, divergence, temperature and surface pressure equations, due to transient eddy flux convergences. (The small contribution from transients in the surface pressure equation is included for completeness.) The diabatic heating is explicitly accumulated during the GCM integration. The tendency due to transients is computed as the residual when the GCM's time-mean flow is substituted into the full GCM equations.

c. *Total forcing*

The linear and steady nonlinear model simulations of the 205 mb zonal wind anomalies, when forced by anomalous diabatic heating as well as the anomalous tendency due to transient eddy fluxes, are shown in Fig. 6 for both the weak and strong anomaly cases. The corresponding 205 mb geopotential height anomalies are shown in Fig. 7. The linear model provides a useful first approximation to the GCM (Fig. 5). The symmetry of the equatorial response about the equator is captured, despite the gross asymmetry of the forcing. The alignment of the zonal wind anomalies with the heating and cooling anomaly centers is also captured, to first approximation, contrary to what one might expect from the response of Gill's simplest steady state model to monopolar localized forcing. The relative magnitude of the equatorial and subtropical wind anomalies is also basically correct.

Upon closer inspection, significant differences between the linear simulation and the GCM are apparent. The linear response is shifted westward with respect to

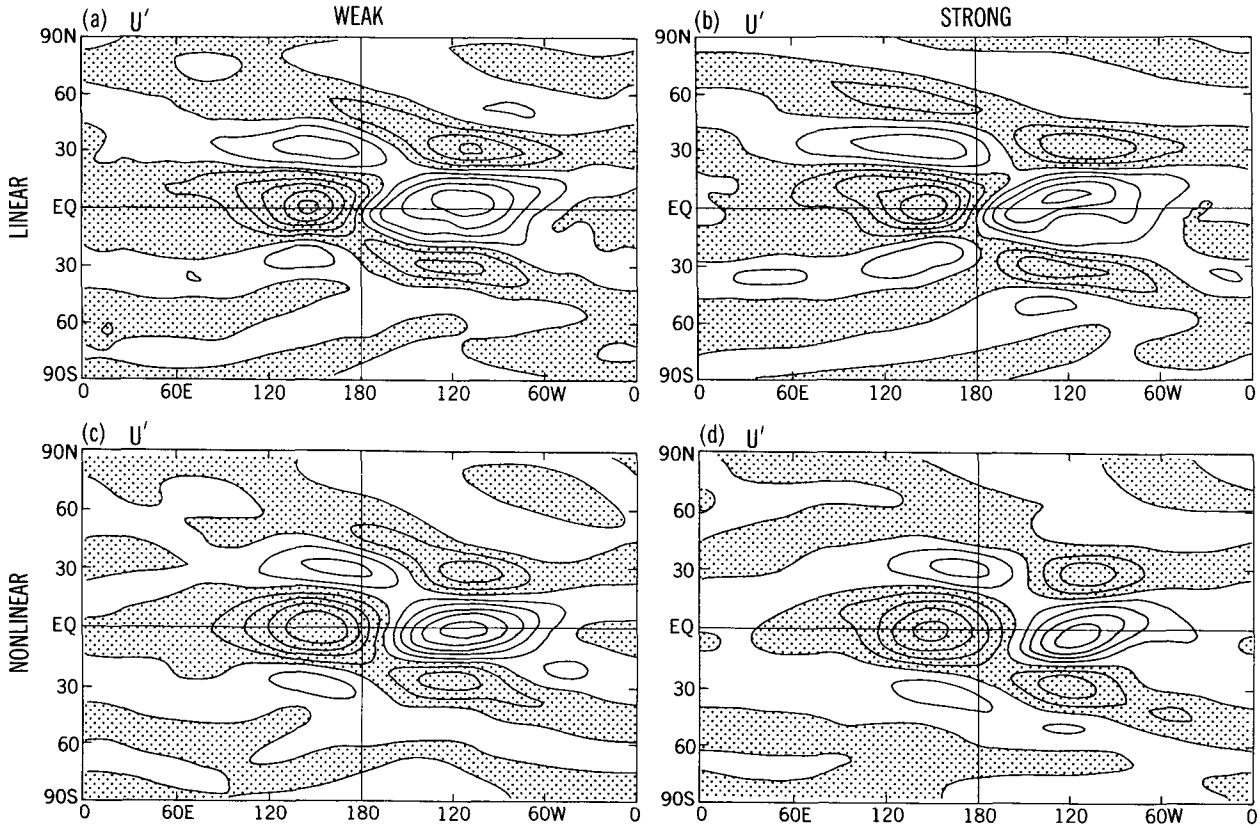

FIG. 6. Linear model eddy zonal wind at 205 mb forced by weak (a) and strong (b) anomaly heating plus transients, and nonlinear model eddy zonal wind at 205 mb forced by weak (c) and strong (d) anomaly heating plus transients. Contour intervals are 2 m s^{-1} for (a) and (c), and 4 m s^{-1} for (b) and (d). Negative values are shaded.

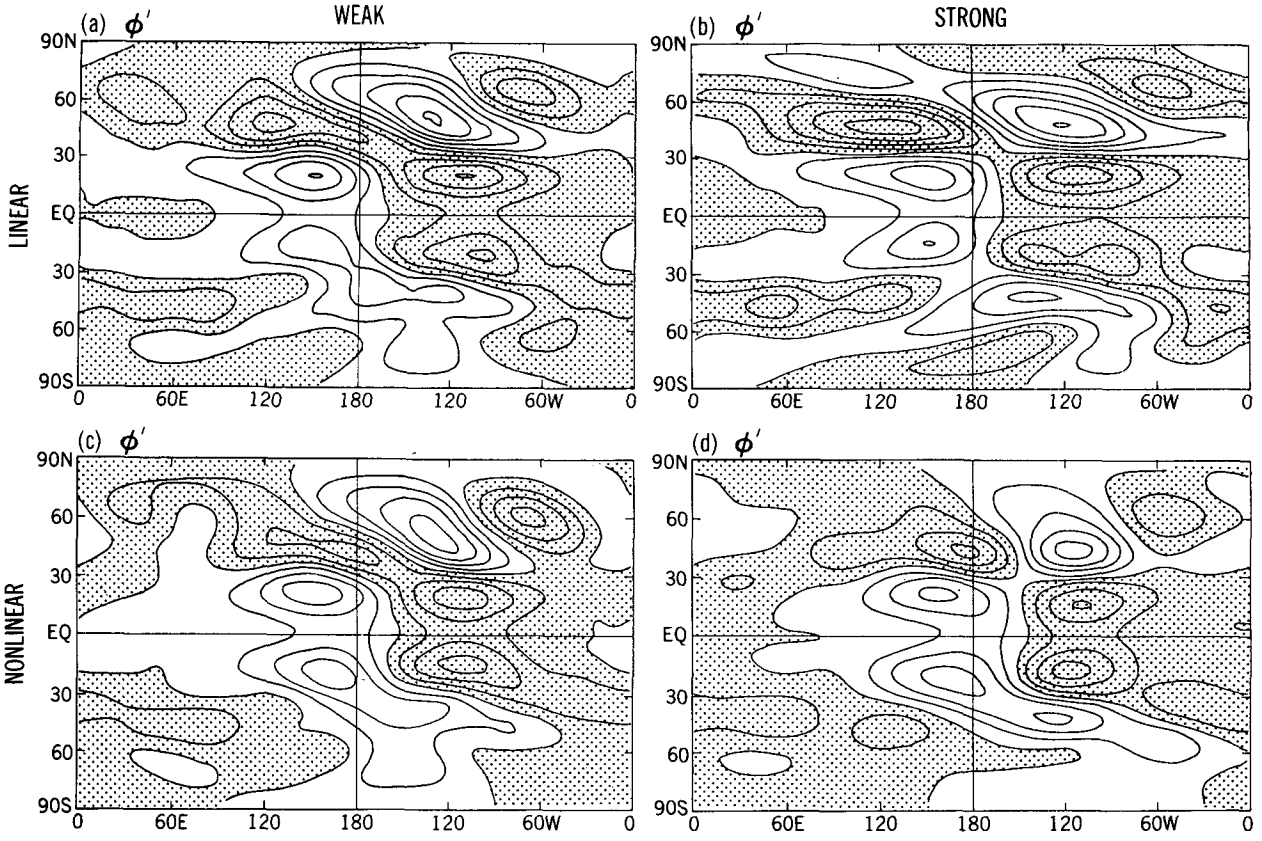

FIG. 7. Same as Fig. 6, but for eddy geopotential. Contour intervals are 10 gpm for weak and 20 gpm for strong anomaly cases, and negative values are shaded.

the GCM, as is most evident in the position of the zero contour in the zonal wind along the equator and in the longitude of the midlatitude geopotential height anomalies. The maximum equatorial westerly anomaly is located north of the equator in Figs. 6a,b, whereas it is south of the equator in the GCM. The extratropical geopotential height pattern is also deformed significantly. Most of these discrepancies between the linear model results and the GCM are reduced by the inclusion of nonlinearity (Figs. 6c,d and Figs. 7c,d). The zero contour in the equatorial wind anomaly is shifted eastward, and the shape of the midlatitude wavetrain improved.

Figure 8 shows the vertical structure of the equatorial zonal wind anomaly in the weak anomaly run of the GCM (a), and in the corresponding linear (b) and steady nonlinear model (c). All three panels show the familiar baroclinic vertical structure. The low level zonal wind anomaly is slightly stronger in the linear model than in the GCM, and the vertical structure of the upper level anomaly differs as well: in the linear model, the upper level easterly anomaly penetrates farther into the midtroposphere than does the westerly anomaly; in the GCM, the opposite is the case. These discrepancies are again reduced by including nonlinearity.

The slight differences between the GCM pattern and that simulated by the steady nonlinear model can be attributed to the fact that the surface Rayleigh friction and sensible heating parameterization scheme do not exactly mimic the GCM's boundary layer fluxes, and to the zonal truncation of the steady nonlinear model. These calculations with the nonlinear model, in which the full heating field and the transient eddy fluxes as generated by the GCM are included as forcing, are essentially consistency checks. The value of the nonlinear model becomes more evident when one simplifies the model or removes part of the forcing, such as the forcing by transient eddy fluxes. To our knowledge, this is the first attempt to diagnose a GCM's time-mean flow with a nonlinear, baroclinic, multilayer steady state model closely based on the GCM's equations of motion. In the present case, the linear model provides a simulation that is adequate for many purposes. The value of the steady nonlinear model should be more evident in a case for which the linear model fails badly.

In order to better appreciate why nonlinearity of the stationary flow is not of great importance, we show in Fig. 9 the total streamfunction and absolute vorticity in the strong anomaly integration at 205 mb. For comparison, we also show the 150 mb flow during northern winter observed during 1983–84. The divergence at

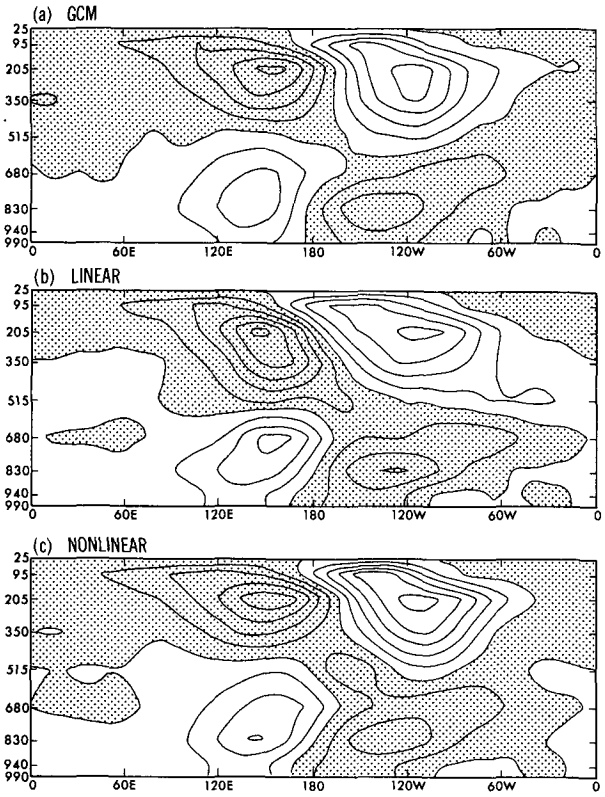

FIG. 8. Longitude-height cross section of equatorial eddy zonal wind in weak anomaly case from GCM (a), linear model (b), and nonlinear model (c). Contour interval is 2 m s^{-1} and negative values are shaded.

this level is shown by the shaded contours superposed on the vorticity plots. The GCM's divergence is weaker than that observed over Indonesia, and the extended region of weak $f + \zeta$ in the winter hemisphere is not present. As a result, the absolute vorticity contours near the equator are more zonal than in the observations. (In fact, because the GCM's heating anomaly is primarily south of the equator, the resulting flow bears a greater resemblance to that over the Amazon rather than over Indonesia and the Pacific.) The absolute vorticity field in the model is not as zonally asymmetric as the observed field, suggesting that a linearization about a zonally symmetric flow is a better approximation for the model than for the atmosphere.

d. Anomalous heating vs. transients

Figure 10 shows the 205 mb eddy zonal wind and geopotential forced by heating in isolation (removing the forcing due to transient eddy fluxes) in the weak anomaly experiment, as simulated with the steady linear and nonlinear models. It is more convenient to use the forcing from the weak anomaly experiment when generating steady nonlinear solutions, because the iteration scheme converges more quickly than for the strong anomaly case. The dynamics of the weak and strong anomaly patterns appear to be very similar, so we lose little by concentrating on the weak anomaly results.

As compared with the linear response to heating plus transients (Fig. 6a), the tropical zonal winds in the linear response to heating in isolation are 1) much stronger (the contour interval is a factor of two larger in Fig. 10a than in Fig. 6a), 2) displaced about 30° longitude to the west, and 3) trapped in a narrower region about the equator. There is clearly strong compensation between anomalies forced by heating and by transients. This compensation is particularly strong in the region of westerlies over the cooling center at 150°W. The maximum westerly anomaly is 28 m s^{-1} in Fig. 10a and 9 m s^{-1} in Fig. 6a. The transients reduce the amplitude and broaden and shift eastward the upper tropospheric equatorial wind anomalies. This is qualitatively similar to the result in Gill's (1980) model when one increases the strength of the damping in the vorticity equation. We return to this point after examining the transients in more detail in section 5.

The nonlinear model result in Fig. 10b confirms the linear model diagnosis. The equatorial westerly anomaly (and, to a much lesser extent, the easterly anomaly) forced by heating in isolation is stronger than that forced by heating plus transients (Fig. 6c), so once again the transients act to damp the response. Note that the strong equatorial westerly anomaly forced by heating in the nonlinear model (Fig. 10b) is shifted to the east as compared with the linear result, so that its position corresponds roughly to that observed in the GCM, although its shape is severely distorted. An eastward shift due to nonlinearity has been discussed by Sardeshmukh and Hoskins (1985) and Hendon (1986) in their simulations of the strong 1982–83 ENSO event. Nonlinearity also strengthens the maximum westerly anomaly (29 m s^{-1} in 10b as compared with 25 m s^{-1} in 10a) and weakens the easterly anomaly (10 m s^{-1} as compared with 16 m s^{-1}). This is to be expected from the increase in cyclonic vorticity in the westerly region, which increases the strength of the vortex stretching for a given vertical velocity field, and the anticyclonic circulation in the region of equatorial easterlies, which reduces the strength of the vorticity source. The fact that the westerlies are already stronger than the easterlies in the linear solution appears to be due to constructive interference in the westerly region between the responses to the positive and negative rainfall anomalies. Once the transients are included, however, the strengths of easterly and westerly anomalies become comparable.

The role played by the transient eddy flux convergence in damping the extratropical wavetrain can be seen clearly in the eddy geopotential height field (Figs. 10c,d). Comparing the wavetrain forced by heating plus transients in the linear model (Fig. 7a) with that forced by heating only (Fig. 10c), we find a very similar pattern differing in amplitude by nearly a factor of two.

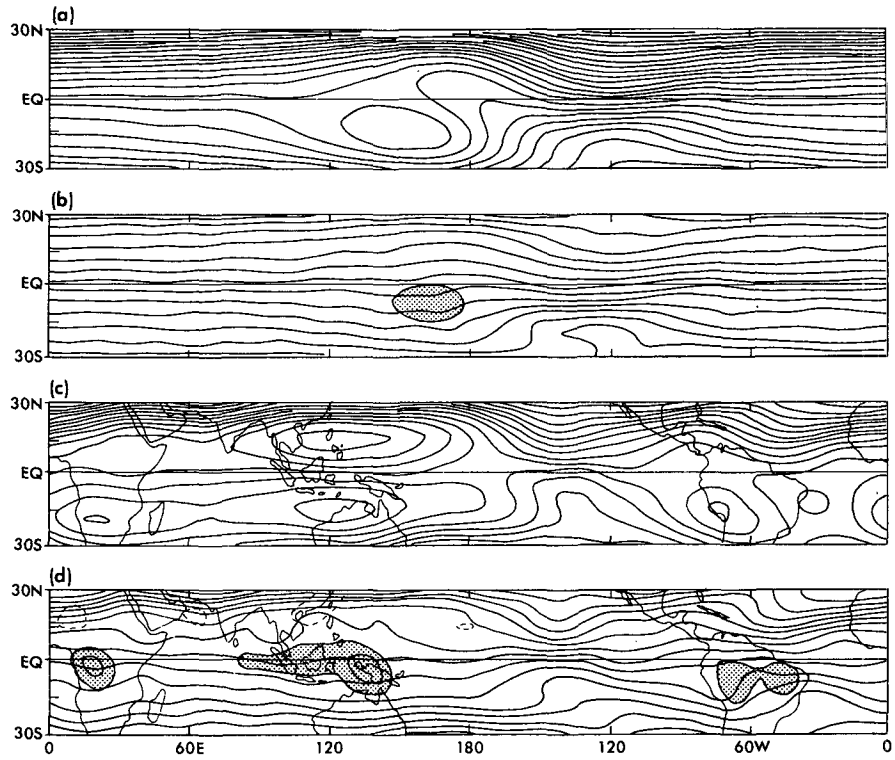

FIG. 9. Contours of streamfunction (a) and absolute vorticity (b) in the latitudinal belt 30°S to 30°N at 205 mb for the strong anomaly experiment. The contour intervals are 5×10^6 m^2 s^{-1} and 1×10^{-5} s^{-1}, respectively. Also shown by shaded contours is the divergence, with a contour interval of 3×10^{-6} s^{-1}. (c) and (d) are the observed streamfunction and absolute vorticity for the northern winter of 1983–84 at 150 mb, taken from Held and Hoskins (1985) and originally computed from ECMWF data by P. Sardeshmukh.

(The contour interval in Fig. 10 is again twice that in Fig. 7.) The Northern Hemisphere extratropical high in Fig. 7a is only 50 gpm while it is nearly 90 gpm in Fig. 10c. Transients are damping the extratropical wavetrain as well as the equatorial winds, in sharp contrast to the positive feedback due to transients found by HLN. The steady nonlinear geopotential response to heating (Fig. 10d) is shifted eastward compared to the linear result. The pattern is similar to the linear prediction, but the lows tend to be stronger and the highs weaker. It is almost exactly in phase with the nonlinear response to total forcing in Fig. 7c, but once again has larger amplitude.

Further separation of the stationary eddy field into parts forced by heating and transients in different regions has been performed with the linear model. Figures 11a,b show the 205 mb eddy geopotential forced by the transients north and south of 30°N, respectively. The transients south of 30°N are generating a Northern Hemispheric wavetrain opposite in phase to that in the total response, and are clearly responsible for the dissipative effect of the transients. The response to the extratropical transients in the Northern Hemisphere is small in comparison. The extratropical transients are not playing a simple dissipative role, but neither are they forcing a wavetrain that bears much resemblance to that in the total response—unlike the model analyzed in HLN. We have decomposed Fig. 11b further to verify that it is the tropical transients, primarily between 20°N and 20°S, and not the transients in the Southern Hemisphere that are responsible for the damping of the northern wavetrain. Furthermore, the upper tropospheric transients in the vorticity equation are responsible for almost all of this effect; lower tropospheric transients and transients in the temperature equation are relatively insignificant.

e. The influence of the modified zonal mean flow

As shown in Fig. 3, there is a significant increase in the zonal mean equatorial upper tropospheric westerlies in the anomaly experiments. In all the linear and nonlinear calculations presented above, we use the zonally averaged basic flow from the corresponding anomaly experiments. We have performed identical calculations using, instead, the zonal mean climate of

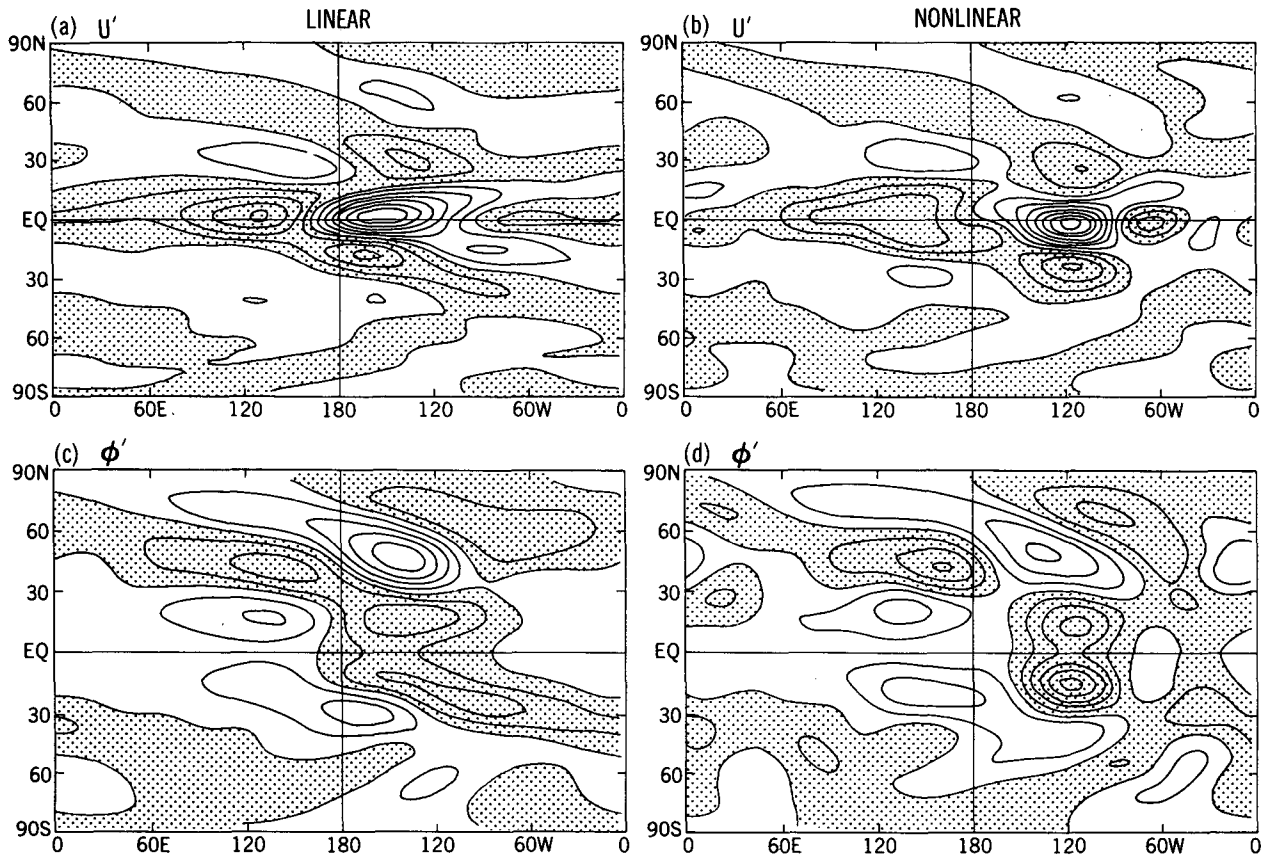

FIG. 10. Linear model eddy zonal wind (a) and geopotential (c), nonlinear model eddy zonal wind (b) and geopotential (d) at 205 mb forced by weak anomaly heating. Contour intervals are 4 m s^{-1} in (a) and (b) and 20 gpm in (c) and (d). Negative values are shaded.

the control run, and find that the differences are relatively small but not entirely negligible. For example, Fig. 12 shows the eddy zonal wind and geopotential produced by the linear model forced by heating plus transients from the small anomaly integration, but with the control basic state. The largest change from Fig. 6a and Fig. 7a is in the region of the easterly anomaly, where the response is weaker by 4 m s^{-1}.

The change in the extratropical geopotential is at most 20 gpm, with the response using the control mean winds being slightly stronger. This effect is contrary to one's intuition that stronger mean westerlies would allow a larger wave to emerge from the tropics, and we return to this point in section 5. The nonlinear simulation (not shown) is somewhat less sensitive to the change in the zonal mean than is the linear result, but the qualitative results are similar: the tropical zonal winds are strengthened by the change in the zonal mean flow generated by the SST anomaly, while the extratropical response is slightly weaker. In any case, the influence of different zonally averaged basic flows on the stationary wave is small compared with the effects of transients.

5. Transients

To help understand the dynamics of these upper tropospheric vorticity transients, we have examined the flow at the $\sigma = 0.205$ level, sampling the GCM's data once per day. Both the transient eddy vorticity fluxes and the stationary eddy response to transient forcing reach their maximum values at this level. Since the lower boundary in this idealized GCM is flat, this σ-level coincides closely with the 205 mb pressure surface, and we ignore the difference between sigma-coordinate and pressure-coordinate vorticity.

The vorticity and streamfunction tendencies are computed as

$$\frac{\partial \bar{\zeta}}{\partial t} = -\nabla \cdot (\overline{\mathbf{V}'\zeta'}), \quad \frac{\partial \bar{\psi}}{\partial t} = \nabla^{-2}\left(\frac{\partial \bar{\zeta}}{\partial t}\right) \qquad (4)$$

where an overbar represents time averaging, and a prime the deviation of the instantaneous value from the time-mean value. The vertical advection and twisting terms are neglected. This explicitly computed tendency is almost identical to that obtained from the full GCM equations as a residual and is used as forcing in our steady state models. (HLN found significant

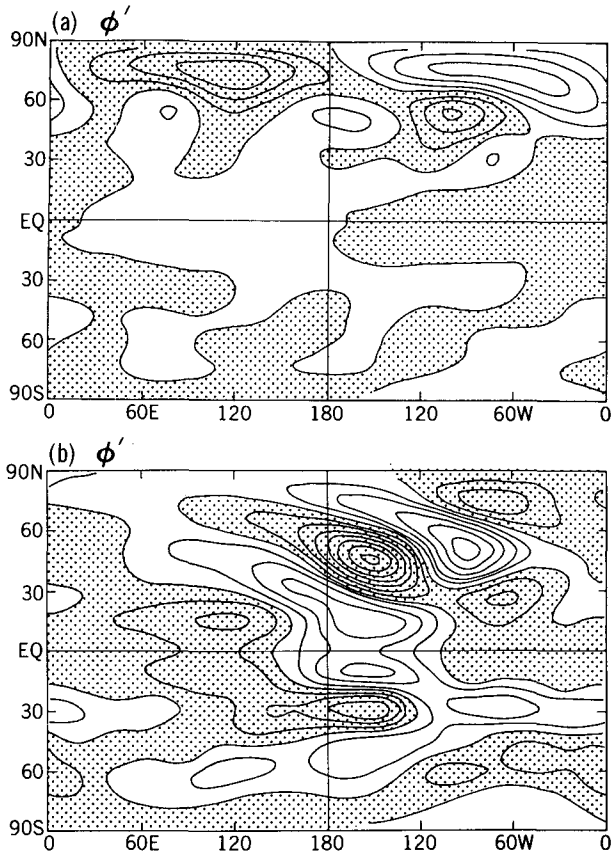

FIG. 11. Eddy geopotential at 205 mb forced by weak anomaly extratropical (a) and tropical (b) transients in the linear model. Contour interval is 10 gpm and negative values are shaded.

differences when making the same comparison, presumably because of the large differences between constant sigma and pressure levels when using realistic topography.)

Figure 13a contains the zonally asymmetric streamfunction tendency due to transient vorticity flux convergence at this level in the strong anomaly GCM experiment. We use the transients from the strong anomaly case because they provide a somewhat clearer picture due to the larger signal to noise ratio. The results for the weak anomaly experiment are qualitatively similar. The data have been Fourier transformed and split into two parts corresponding to periods less than and greater than 10 days. These two parts are displayed in Figs. 13b,c. Most of the structures in Fig. 13 are confined between 30°N and 30°S, consistent with the linear model results for tropical and extratropical transient forcing in Fig. 11. The streamfunction tendencies show a strong cyclone (anticyclone) pair straddling the equator at approximately the same longitude as the warm (cold) SST anomaly. The corresponding zonal wind tendencies are almost exactly out of phase with the GCM's zonal wind anomalies on the equator and in the subtropics (see Fig. 5a). Over the cold water in particular, the maximum in the equatorial zonal wind tendency is displaced south of the equator, just as is the GCM's zonal wind anomaly in this region. The tropical transients are again seen to be damping the response, as observed in our linear and nonlinear diagnoses.

The contributions of high and low frequency transients are similar in structure in the tropics, each contributing about half of the total. The high frequencies are somewhat more dominant in the Northern Hemisphere. Although it is not very clear with the contour interval in Fig. 13, the contributions from high and low frequencies have a very different structure in the extratropical Northern Hemisphere, generally being of opposite sign.

To relate the zonal wind tendency with changes in the characteristics of eddy propagation, it is useful to plot the vector field:

$$\mathbf{E} = \left(\frac{\overline{v'^2} - \overline{u'^2}}{2}, -\overline{u'v'} \right). \tag{5}$$

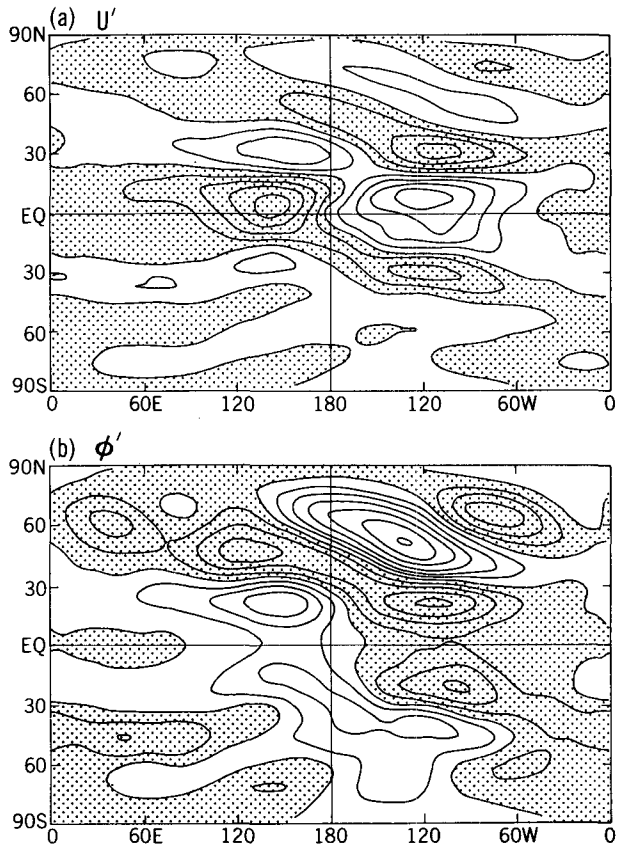

FIG. 12. Eddy zonal wind (a) and geopotential (b) at 205 mb forced by weak anomaly total forcing in the linear model using control zonal mean basic state. Contour intervals are 2 m s^{-1} in (a) and 10 gpm in (b). Negative values are shaded.

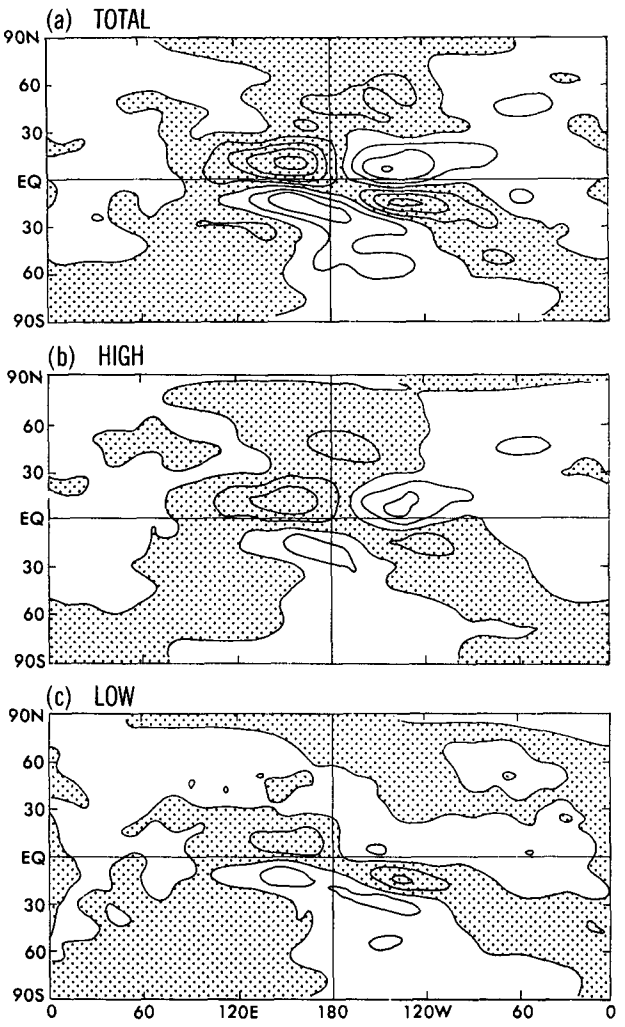

FIG. 13. Eddy streamfunction tendency due to strong anomaly GCM transient vorticity flux divergence computed from daily sampled data (a), high-pass filted data (b) and low-pass filted data (c). Contour interval is 1×10^6 m^2 s^{-1} day^{-1}. Negative values are shaded.

The vector **E** points in the direction of the group velocity with respect to the environment, if the eddy statistics are dominated by barotropic Rossby waves with a definite frequency and local wavenumber (Hoskins et al. 1983; Plumb 1986). (For baroclinic waves, Plumb shows that one must include a term proportional to the temperature variance in the zonal component; since our interest is primarily in the low latitude transients, for which the temperature variance is small, and since we have already determined that the transients in the vorticity equation are of paramount importance, we have chosen the simple barotropic form that is closely related to the vorticity forcing.) If one eliminates the factor of ½ in the first component, then $\nabla \cdot \mathbf{E}$ approximates the zonal wind acceleration (deceleration) that acting alone, without any corresponding meridional wind tendency, would produce the correct vorticity tendency. Figure 14 contains plots of (a) the total **E** at 205 mb in the strong anomaly experiment, (b) the zonally asymmetric **E** in the strong anomaly experiment, (c) the contribution to (b) from high frequency eddies, and (d) the contribution from low frequencies. The time-mean zonal wind field from the GCM is also contoured in each case.

In (a) and (b) one clearly sees a divergence out of the region of mean easterlies and convergence into the region of strong westerlies along the equator, consistent with the mean flow tendencies inferred from Fig. 13. In both cases, it is the meridional convergence, associated with meridional wave propagation, rather than zonal convergence that is dominant. There is anomalous poleward wave propagation out of the tropical easterlies region and equatorward propagation into the tropical westerlies.

In the extratropics, the **E**-vector anomalies are more zonally oriented. It is known (e.g., Fig. 6 in Hoskins et al. 1983) that $v'^2 \gg u'^2$ for high frequency storm-track eddies, resulting in eastward pointing **E**-vectors. For low-frequency eddies, u'^2 dominates, and **E**-vectors are westward. Therefore, Fig. 14c can be interpreted as an equatorward shift of the high frequency variance near the Northern Hemisphere jet maximum, with larger values on the southern flank of the jet and smaller values to the north. One gets the impression of enhanced propagation away from the region of increased baroclinic activity south of the jet, partly polewards and partly equatorwards through the westerly wind waveguide. One sees a weaker increase in the high pass variance north of the jet in the Southern Hemisphere. However, the equatorward propagation into the equatorial westerly maximum from the south is just as large as its northern counterpart at high frequencies and has, in addition, a large low-frequency component, suggesting that different mechanisms may be dominant in the two hemispheres.

Another clear signal in the low-frequency statistics is the westward **E**-vector in the jet exit region of the Northern Hemisphere. This is the pattern expected from barotropic instability of the asymmetric jet (Simmons et al. 1983; Wallace and Lau 1985), and is very distinct from the high frequency contribution in the same region, consistent with the different streamfunction tendencies in Fig. 13c at extratropical latitudes.

In order to understand the dissipative effects of transients on the stationary eddy in the GCM, one has to understand the dynamics underlying the convergence of eddy activity into the tropical westerlies and divergence out of the tropical easterlies. There are at least three possibilities:

1) The easterlies (westerlies) are located directly above the region of increased (reduced) convection. There should be more poleward propagating waves

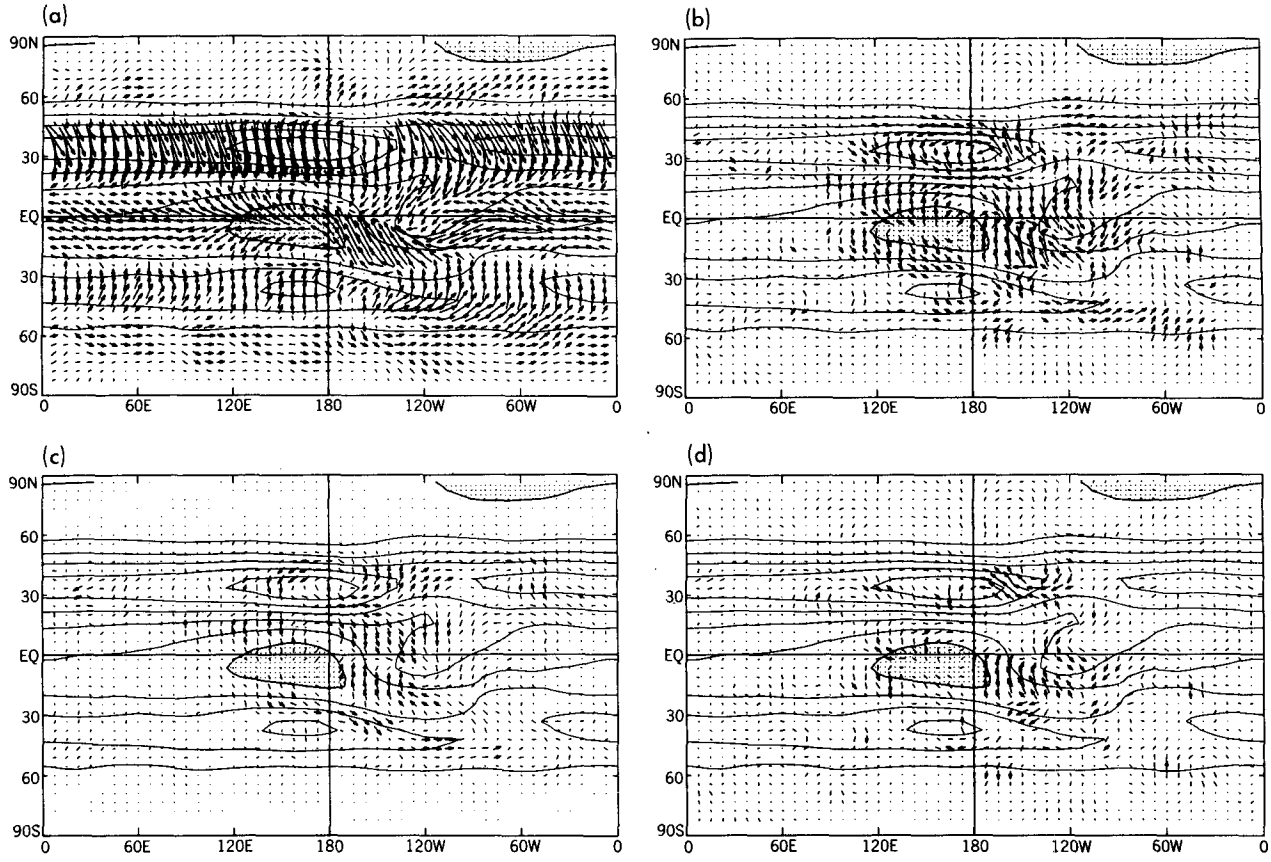

FIG. 14. Total E-vector (defined as in text) (a), eddy E-vector (b) calculated from strong anomaly GCM daily sampled data, and eddy E-vector computed from high-pass filted data (c) and low-pass filted data (d) along with the time-averaged zonal wind field. Contour interval for zonal wind is 10 m s^{-1} and negative values are shaded. The scale of the arrow is as follows: The length of 30° in longitude and latitude represents 80 m^2 s^{-2}.

generated by time-dependent convection at the longitude of the easterlies than in the control integration, and less at the longitude of the westerlies.

2) The westerlies allow more extratropical wave activity to propagate into the deep tropics before dissipating, while the easterlies block this propagation.

3) Barotropic instability of the strongly asymmetric flow in the tropics could produce transients that act to damp the eddy zonal winds along the equator.

To address the third possibility, we have examined a time dependent, fully nonlinear barotropic model, in which the divergence and the zonal mean zonal flow are fixed at the time mean GCM values of the strong anomaly experiment at 205 mb, as in Held and Kang (1987). The equation reads

$$\frac{\partial \zeta'}{\partial t} = -\nabla \cdot [(f + \zeta)\mathbf{V}]' - \kappa\zeta' + \upsilon\nabla^4\zeta', \quad \mathbf{V} = \mathbf{V}_\psi + \mathbf{V}_x \tag{6}$$

where a prime represents the deviation from the zonal mean and $\mathbf{V}_x$ is the prescribed irrotational part of the flow. The Rayleigh friction controls the energy level of the eddies that are generated through barotropic instability. Its strength is arbitrary; we have chosen the relatively low value of $\kappa = (30 \text{ day})^{-1}$. The biharmonic diffusion coefficient is taken from the GCM: $\upsilon = 1 \times 10^{16}$ m^4 s^{-1}. This equation is spectrally transformed on the sphere using spherical harmonics and truncated rhomboidally to wavenumber 15. The equation is integrated for 1000 days.

The time-averaged zonal wind and E-vector field are plotted in Fig. 15. All frequencies are included in the E-vector. The time–mean zonal wind in Fig. 15 shows a similar pattern as the GCM's zonal flow in Fig. 14, although the stationary eddy amplitudes are stronger. Equatorial easterlies and westerlies are generated at roughly the same longitudes as in the GCM, although the westerlies are displaced eastward. Comparing Fig. 15 with Fig. 14d, we notice similar structures in the jet exit regions, particularly in the Northern Hemisphere, as anticipated from the barotropic instability of the extratropical mean flow. However, in the tropics there is no counterpart of the large signal in

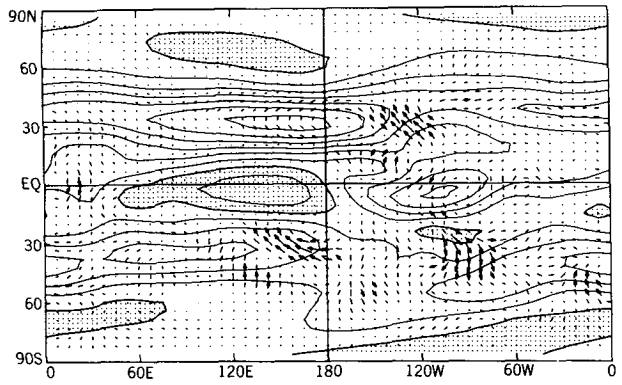

FIG. 15. E-vector calculated from daily sampled data from the time-dependent barotropic model integration, along with the time-averaged zonal wind field produced by that model. Contour interval for time-mean zonal wind is 10 m s^{-1} and negative values are shaded. The scale for the arrow is the same as in Fig. 14.

Fig. 14, despite the fact that the barotropic model has produced larger tropical stationary wave amplitudes, which should enhance any barotropic instabilities. This result demonstrates that the tropical features in Figs. 14c,d cannot be caused by barotropic instability. Note also that the larger stationary wave amplitudes obtained from the barotropic model are consistent with the fact that it omits an important source of dissipation.

It is more difficult to judge the relative importance of the two remaining possibilities listed above: the effects of extratropical eddies penetrating into the tropics and of eddies generated by time-dependent convection. The zonal wind acceleration in the region of tropical easterlies, for example, could be due either to an enhancement of outward propagation due to increased convection, or a reduction in the inward propagation due to the effect of the easterlies on meridional wave propagation. We have not as yet tried to separate these two effects. Our impression from Fig. 13a is that the convective contribution is more important. If the effects of extratropical wave penetration into the tropics were dominant, it would be surprising that the tendency due to transients is roughly symmetric about the equator.

It is clear that, even in this idealized GCM, the effects of transient eddies on the climatic response are complex. It may be necessary to study a simpler model, in which the time-dependence of the tropical heating can be suppressed, to make a clean separation between extratropical and tropical sources of anomalous eddy fluxes.

Even without a clear understanding of the underlying dynamics, one is tempted to replace the tropical transients by simple damping. From inspection of the streamfunction or zonal wind tendencies we estimate a damping time scale of approximately four days in the tropical upper troposphere. Figure 16a is the zonal wind anomaly predicted by the linear model when forced by the weak anomaly heating, with the inclusion of a 4-day damping of vorticity in the tropical upper troposphere. (The damping is included only equatorward of 30° and at the 0.205, 0.350 and 0.515 σ levels; explicit forcing by transients is omitted entirely.) The amplitude of the equatorial wind anomalies in Fig. 16a is comparable to that in Fig. 6a; however, the subtropical winds are much weaker. Inspection of the geopotential (not shown) confirms that the extratropical response is now much too small. Inclusion of the extratropical transients as explicit forcing increases this amplitude somewhat, but the resulting pattern does not resemble the GCM flow.

A similar nonlinear calculation with the forcing by transients replaced by 4-day damping of vorticity in the tropics is shown in Fig. 16b. One finds that the nonlinearity shifts the westerly wind anomaly eastward to its correct position, while increasing the strength of the westerlies and decreasing the strength of the easterlies. These are similar to the effects seen in Fig. 10, but they are smaller due to the damping.

Using this dissipative model forced by heating only,

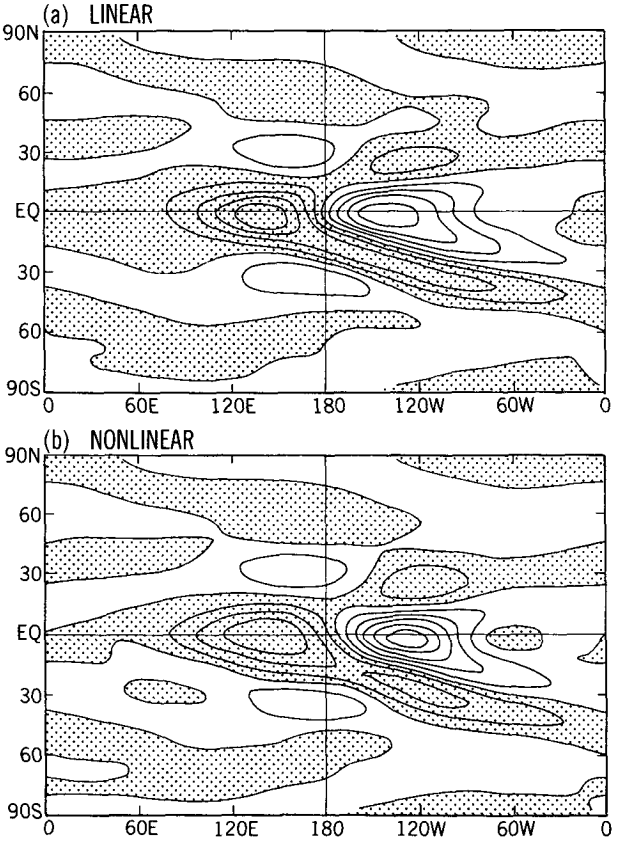

FIG. 16. Eddy zonal wind at 205 mb forced by weak anomaly heating in a linear (a) and nonlinear (b) model with a 4-day damping at level 3, 4, 5 and between 30°S and 30°N. Contour interval is 2 m s^{-1} and negative values are shaded.

we have repeated the calculations testing the sensitivity of the stationary eddies to the change in the zonal mean wind. The only noteworthy result is that the amplitude of the extratropical wavetrain now increases as the mean equatorial westerlies increase in strength. The meridional group velocity of stationary Rossby waves increases as the mean westerlies increase; as a result there is less time to damp the waves, and they emerge from the tropics with larger amplitude (although still too small compared with the GCM). In the calculations described in Fig. 12, there evidently is not enough dissipation in the tropics for this argument to be relevant, and the amplitude of the extratropical wavetrain actually decreases as $\bar{u}$ increases. This result serves to stress the importance of parameterizing the effects of transients before reaching any conclusions about the sensitivity of the stationary eddies.

6. Comparison with HLN

The difference between the effects of transients on the stationary eddy pattern in this GCM and the effects found by HLN is dramatic. To check that this difference is not caused by differences in the linear models used to determine the effects of transients, we have repeated the calculations in HLN with the linear model used here. We find that some of the results in HLN are sensitive to the large tropical damping included in their calculations; however, the result that the transients provide strong positive feedback on the extratropical response in the GCM analyzed by HLN is robust.

If we include the same strong damping as is used by HLN in the fully spectral linear model used for this study, and reanalyze the GCM calculations that they discuss, nearly identical results to those in HLN are obtained: the direct stationary eddy response to tropical heating is small but generally of the correct phase, while the transients provide a strong enough positive feedback that the total linear response to heating plus transients is similar to that of the GCM. As the tropical damping is reduced in strength, the direct response to heating increases so that in isolation it provides a somewhat better simulation of the GCM, but the response to the transients also increases, resulting in a stationary eddy that is much too large (by a factor of two when the tropical damping is removed entirely). At face value, this implies that nonlinearity is more important in the realistic GCM's simulation of the El Niño response than in the present idealized GCM's response to the SST anomaly of Fig. 1. We have been reluctant to apply the steady nonlinear model to the case studied by HLN, since the response being analyzed is a composite of several events simulated by the GCM with different SST distributions. The dynamics of a composite would be difficult to interpret if the response were, in fact, nonlinear.

The extratropical transients in HLN provide a strong positive feedback on the stationary eddy, while the extratropical transients here have little effect on the response. Our working hypothesis is that a storm track that is strongly zonally asymmetric responds very differently to forcing from the tropics than does an initially symmetric storm track. The tropical transients also have a significant effect in HLN, although it is not a dissipative one of the sort found here. A strong easterly anomaly is produced across the Pacific by the El-Niño boundary conditions, and penetration of wave activity into the tropics from the north appears to be suppressed; but the main result is to displace the deceleration due to the waves poleward, broadening the easterly wind anomaly, rather than weakening it in a symmetrical fashion about the equator. Why transients in the tropics should behave so differently in the two cases is obscure.

7. Conclusions

The upper tropospheric response to a tropical SST anomaly in an idealized GCM has been analyzed using linear and nonlinear steady state models as diagnostic tools. The control GCM experiment has a zonally symmetric climate. The response is expected to differ from that obtained using a more realistic control climate not only because the interaction between the preexisting stationary eddy and the forced wave may be important in the realistic case, but also because a zonally asymmetric storm track may respond differently to the tropical forcing than an initially symmetric storm track; resulting in a qualitatively different feedback onto the time-mean response. This study can be thought of as preparatory to a similar analysis using a more realistic control climate. It should also be thought of as preparatory to similar calculations with higher resolution models with more convincing eddy dynamics.

The two GCM anomaly experiments produce a heating field that is approximately linear in the amplitude of the SST anomaly. In the large anomaly case, the precipitation has dropped to nearly zero over the cold water, indicating that the heating field would be less linear if the amplitude of the SST anomaly were increased further. The response of the mean flow to this heating field is also very linear, both in the tropics and the extratropics: the two patterns are almost identical, differing in amplitude by a factor of two. The linear steady state model is quite successful in simulating this pattern when forced by the heating field and the anomalous transient eddy fluxes, confirming this impression of linearity. Both the symmetry of the response about the equator, and the alignment in longitude between the SST extrema and the zonal wind response are captured by this linear model. Furthermore, a fully nonlinear steady state model produces a flow differing only in some details from the linear

model; the tropical and extratropical flow patterns are shifted eastward slightly, and the equatorial westerlies (easterlies) are strengthened (weakened). While there is a significant increase in the zonal mean zonal flow in the anomaly experiments, the effect of this change on the response of the steady state models is relatively minor.

A much more complicated picture emerges when one separates the response to the heating from the response to the anomalous transient eddy fluxes. The response to heating in isolation is similar in structure to the GCM eddy, but it is too strong in both tropical and extratropical latitudes, by roughly a factor of two. The effect of the transients, particularly the anomalous transient vorticity fluxes in the tropical upper troposphere, is to damp the response. The same conclusion is reached using either the linear or the nonlinear steady state model. If this damping effect were absent, these steady models suggest that the response to the heating would be much more nonlinear. An attempt at mimicking the effects of these transients within the tropics by including a uniform damping on the upper tropospheric vorticity is successful in simulating the amplitude of the equatorial zonal winds, and, especially when using the steady nonlinear model, the structure of these winds as well. However, this procedure is too crude to obtain the correct extratropical response.

Inspection of the E-vectors associated with the upper tropospheric transients indicates that the damping within the tropics is due to modified meridional rather than zonal transient eddy propagation. The possibility that barotropic instability within the tropics is a source of the damping is ruled out with a nonlinear time-dependent barotropic model. However, we have not attempted to separate the effects of anomalous wave radiation out of the tropics, which are due to shifts in the time-dependent tropical heating field, from the effects of anomalous propagation of midlatitude disturbances into the tropics, which are due to the changing zonal wind field forced by the mean heating. Outside of the tropics, one does see the signature of barotropic instability in the jet exit region of the winter hemisphere, and one also sees an equatorward shift in the storm track at the longitude of the heat source, but these play a relatively minor role in determining the time-mean flow. The differences between these results and those of HLN suggest that a strongly asymmetric storm track, with a well-defined baroclinic source and barotropic decay regions, is necessary before significant positive feedback can occur. Similar studies—but using a zonally asymmetric control climate—will be needed to clarify this problem.

Acknowledgments. We acknowledge helpful conversations with E. Schneider and P. Valdes on numerical techniques for linear and nonlinear stationary wave problems. The advice of K. Cook was also very helpful in setting up the GCM integrations. One of the authors (MFT) was supported by NOAA Grant NA87EAD00039.

APPENDIX

Steady Linear and Nonlinear Models

a. Linear model with symmetric basic state

The steady, linear, baroclinic model follows the GCM in using σ ($\sigma = P/P_*$, where P_* is surface pressure) as vertical coordinate. There are prognostic equations for the vorticity (ζ), divergence (D), temperature (T), and log surface pressure ($\ln P_*$), plus the hydrostatic and mass continuity equations that determine the geopotential (ϕ) and the vertical velocity ($\dot{\sigma}$). The zonal (u) and meridional (v) wind components can be determined from steam function (ψ) and velocity potential (χ):

$$u = -\frac{\partial\psi}{a\partial\theta} + \frac{\partial\chi}{a\cos\theta\partial\lambda}, \qquad v = \frac{\partial\psi}{a\cos\theta\partial\lambda} + \frac{\partial\chi}{a\partial\theta}$$

and $\psi = \nabla^{-2}\zeta$, $\chi = \nabla^{-2}D$.

Define $U = u\cos\theta$, $V = v\cos\theta$ and use bar to represent the zonal mean basic state about which we linearize the GCM equations, and use prime to represent the deviation from this basic state. In the steady state, we obtain the following equations:

$$0 = -\frac{1}{a\cos^2\theta}\left\{\frac{\partial A'}{\partial\lambda} + \cos\theta\frac{\partial B'}{\partial\theta}\right\} + F'_\zeta - \nu\nabla^4\zeta' \quad \text{(A1)}$$

$$0 = \frac{1}{a\cos^2\theta}\left\{\frac{\partial B'}{\partial\lambda} - \cos\theta\frac{\partial A'}{\partial\theta}\right\} - \nabla^2 E' - \nabla^2\phi' + F'_D - \nu\nabla^4 D' \quad \text{(A2)}$$

where

$$A' = U'(f+\bar{\zeta}) + \bar{U}\zeta' + \frac{R\bar{T}}{a}\cos\theta\frac{\partial(\ln P_*)'}{\partial\theta} + \frac{RT'}{a}\cos\theta\frac{\partial\overline{(\ln P_*)}}{\partial\theta} + \bar{\dot{\sigma}}\frac{\partial V'}{\partial\sigma} + \dot{\sigma}'\frac{\partial\bar{V}}{\partial\sigma}$$

$$B' = V'(f+\bar{\zeta}) + \bar{V}\zeta' - \frac{R\bar{T}}{a}\frac{\partial(\ln P_*)'}{\partial\lambda} - \bar{\dot{\sigma}}\frac{\partial U'}{\partial\sigma} - \dot{\sigma}'\frac{\partial\bar{U}}{\partial\sigma}$$

$$E' = \frac{U'\bar{U} + V'\bar{V}}{\cos^2\theta}$$

$$0 = -\frac{1}{a\cos^2\theta} \times \left\{\frac{\partial}{\partial\lambda}(\bar{U}T' + \bar{T}U') + \cos\theta\frac{\partial}{\partial\theta}(\bar{V}T' + \bar{T}V')\right\}$$

$$+ \bar{T}D' + \bar{D}T' + \frac{\kappa\bar{T}}{\sigma}\dot{\sigma}' + \frac{\kappa T'}{\sigma}\bar{\dot{\sigma}} - \bar{\dot{\sigma}}\frac{\partial T'}{\partial\sigma} - \dot{\sigma}'\frac{\partial\bar{T}}{\partial\sigma}$$
$$+ \frac{\kappa\bar{T}}{\cos\theta}\left\{\frac{\bar{U}}{a\cos\theta}\frac{\partial(\ln P_*)'}{\partial\lambda} + \frac{\bar{V}}{a}\frac{\partial(\ln P_*)'}{\partial\theta} + \frac{V'}{a}\frac{\partial\overline{(\ln P_*)}}{\partial\theta}\right\} + \frac{\kappa T'}{\cos\theta}\frac{\bar{V}}{a}\frac{\partial\overline{(\ln P_*)}}{\partial\theta}$$
$$+ F'_T - \nu\nabla^4 T' \quad \text{(A3)}$$

$$\frac{\partial\phi'}{\partial\sigma} + \frac{RT'}{\sigma} = 0 \quad \text{(A4)}$$

$$\frac{\partial\dot{\sigma}'}{\partial\sigma} + \frac{\bar{U}}{a\cos^2\theta}\frac{\partial(\ln P_*)'}{\partial\lambda} + \frac{\bar{V}}{a\cos\theta}\frac{\partial(\ln P_*)'}{\partial\theta} + \frac{V'}{a\cos\theta}\frac{\partial\overline{(\ln P_*)}}{\partial\theta} + D' = 0$$

$$0 = -\frac{\bar{\bar{U}}}{a\cos^2\theta}\frac{\partial(\ln P_*)'}{\partial\lambda} - \frac{\bar{\bar{V}}}{a\cos\theta}\frac{\partial(\ln P_*)'}{\partial\theta} - \frac{\tilde{V}'}{a\cos\theta}\frac{\partial\overline{(\ln P_*)}}{\partial\theta} - \tilde{D}' + F'_{P_*}. \quad \text{(A6)}$$

The functions F'_ζ, F'_D, F'_T and F'_{P_*} are the forcing, while orography, if present, enters through the lower boundary condition on ϕ. A tilde indicates a vertically averaged quantity.

Equations (A1)–(A6) are finite differenced in the vertical and spectrally transformed in the horizontal precisely as in the GCM to be analyzed. There are nine sigma levels in the vertical and both eddy and zonal mean variables are spectrally truncated at rhomboidal wavenumber 15 (R15) on the sphere; for example,

$$\zeta'(\lambda,\theta,\sigma) = \sum_{m=1}^{15}\sum_{l=|m|}^{|m|+15}\zeta_l^{\,0}(\sigma)P_l^{\,0}(\sin\theta)e^{im\lambda},$$
$$\bar{\zeta}(\theta,\sigma) = \sum_{l=0}^{15}\overline{\zeta_l^{\,0}}(\sigma)P_l^{\,0}(\sin\theta). \quad \text{(A7)}$$

The equations are separable in zonal wave number m. For each m, there are $k = 9$ vertical levels and $n = 16$ meridional wave numbers for each variable, except for surface pressure. Counting ϕ and $\dot{\sigma}$ as independent variables, there are $(5 \times 9 + 1) \times 16 = 736$ complex variables for each complex zonal wave component. The matrix form of the linear model reads

$$\mathbf{A}_m\mathbf{X}_m = \mathbf{B}_m \quad m = 1, 2, \cdots, 15 \quad \text{(A8)}$$

where $\mathbf{A}_m$ is a 736×736 complex matrix, $\mathbf{X}_m$ is the unknown, and $\mathbf{B}_m$ is the forcing vector.

The treatment of ϕ and $\dot{\sigma}$ as independent variables follows Schneider (1989) and has the consequence that when (A1)–(A6) are finite differenced in the vertical, the variables are only coupled to nearest-neighbors, except for the surface pressure, which is coupled to all vertical levels. In fact, $\mathbf{A}_m$ has the following structure:

$$\mathbf{A}_m = \begin{bmatrix} \mathbf{D}_1 & \mathbf{F}_1 & 0 & 0 & 0 & 0 & 0 & 0 & 0 & \mathbf{H}_1 \\ \mathbf{E}_2 & \mathbf{D}_2 & \mathbf{F}_2 & 0 & 0 & 0 & 0 & 0 & 0 & \mathbf{H}_2 \\ 0 & \mathbf{E}_3 & \mathbf{D}_3 & \mathbf{F}_3 & 0 & 0 & 0 & 0 & 0 & \mathbf{H}_3 \\ 0 & 0 & \mathbf{E}_4 & \mathbf{D}_4 & \mathbf{F}_4 & 0 & 0 & 0 & 0 & \mathbf{H}_4 \\ 0 & 0 & 0 & \mathbf{E}_5 & \mathbf{D}_5 & \mathbf{F}_5 & 0 & 0 & 0 & \mathbf{H}_5 \\ 0 & 0 & 0 & 0 & \mathbf{E}_6 & \mathbf{D}_6 & \mathbf{F}_6 & 0 & 0 & \mathbf{H}_6 \\ 0 & 0 & 0 & 0 & 0 & \mathbf{E}_7 & \mathbf{D}_7 & \mathbf{F}_7 & 0 & \mathbf{H}_7 \\ 0 & 0 & 0 & 0 & 0 & 0 & \mathbf{E}_8 & \mathbf{D}_8 & \mathbf{F}_8 & \mathbf{H}_8 \\ 0 & 0 & 0 & 0 & 0 & 0 & 0 & \mathbf{E}_9 & \mathbf{D}_9 & \mathbf{H}_9 \\ \mathbf{G}_1 & \mathbf{G}_2 & \mathbf{G}_3 & \mathbf{G}_4 & \mathbf{G}_5 & \mathbf{G}_6 & \mathbf{G}_7 & \mathbf{G}_8 & \mathbf{G}_9 & \mathbf{D}_{10} \end{bmatrix}.$$

The three diagonal submatrices $\mathbf{D}_k$, $\mathbf{E}_k$, and $\mathbf{F}_k$ ($k = 1, \cdots 9$) are 80×80, the upper boundary blocks $\mathbf{H}_k$ are 80×16, the lower boundary blocks $\mathbf{G}_k$ are 16×80, and the lower right corner component $\mathbf{D}_{10}$ is a 16×16 matrix.

The sparseness of the matrix allows one to save in memory and cpu time. We use a block **L–U** decomposition in which $\mathbf{A}_m$ is decomposed into the product of lower and upper block triangular matrices:

$$\mathbf{A}_m = \mathbf{L}_m\mathbf{U}_m \quad \text{(A9)}$$

where,

$$\mathbf{L}_m = \begin{bmatrix} \mathbf{I} & 0 & 0 & 0 & 0 & 0 & 0 & 0 & 0 & 0 \\ \mathbf{P}_2 & \mathbf{I} & 0 & 0 & 0 & 0 & 0 & 0 & 0 & 0 \\ 0 & \mathbf{P}_3 & \mathbf{I} & 0 & 0 & 0 & 0 & 0 & 0 & 0 \\ 0 & 0 & \mathbf{P}_4 & \mathbf{I} & 0 & 0 & 0 & 0 & 0 & 0 \\ 0 & 0 & 0 & \mathbf{P}_5 & \mathbf{I} & 0 & 0 & 0 & 0 & 0 \\ 0 & 0 & 0 & 0 & \mathbf{P}_6 & \mathbf{I} & 0 & 0 & 0 & 0 \\ 0 & 0 & 0 & 0 & 0 & \mathbf{P}_7 & \mathbf{I} & 0 & 0 & 0 \\ 0 & 0 & 0 & 0 & 0 & 0 & \mathbf{P}_8 & \mathbf{I} & 0 & 0 \\ 0 & 0 & 0 & 0 & 0 & 0 & 0 & \mathbf{P}_9 & \mathbf{I} & 0 \\ \mathbf{Q}_1 & \mathbf{Q}_2 & \mathbf{Q}_3 & \mathbf{Q}_4 & \mathbf{Q}_5 & \mathbf{Q}_6 & \mathbf{Q}_7 & \mathbf{Q}_8 & \mathbf{Q}_9 & \mathbf{I} \end{bmatrix}$$

and

$$\mathbf{U}_m = \begin{bmatrix} \mathbf{R}_1 & \mathbf{U}_1 & 0 & 0 & 0 & 0 & 0 & 0 & 0 & \mathbf{S}_1 \\ 0 & \mathbf{R}_2 & \mathbf{U}_2 & 0 & 0 & 0 & 0 & 0 & 0 & \mathbf{S}_2 \\ 0 & 0 & \mathbf{R}_3 & \mathbf{U}_3 & 0 & 0 & 0 & 0 & 0 & \mathbf{S}_3 \\ 0 & 0 & 0 & \mathbf{R}_4 & \mathbf{U}_4 & 0 & 0 & 0 & 0 & \mathbf{S}_4 \\ 0 & 0 & 0 & 0 & \mathbf{R}_5 & \mathbf{U}_5 & 0 & 0 & 0 & \mathbf{S}_5 \\ 0 & 0 & 0 & 0 & 0 & \mathbf{R}_6 & \mathbf{U}_6 & 0 & 0 & \mathbf{S}_6 \\ 0 & 0 & 0 & 0 & 0 & 0 & \mathbf{R}_7 & \mathbf{U}_7 & 0 & \mathbf{S}_7 \\ 0 & 0 & 0 & 0 & 0 & 0 & 0 & \mathbf{R}_8 & \mathbf{U}_8 & \mathbf{S}_8 \\ 0 & 0 & 0 & 0 & 0 & 0 & 0 & 0 & \mathbf{R}_9 & \mathbf{S}_9 \\ 0 & 0 & 0 & 0 & 0 & 0 & 0 & 0 & 0 & \mathbf{R}_{10} \end{bmatrix}.$$

To obtain the submatrices within $\mathbf{L}_m$ and $\mathbf{U}_m$, first set

$$\mathbf{U}_k = \mathbf{F}_k, \quad k = 1, \cdots, 8$$

and

$$\mathbf{R}_1 = \mathbf{D}_1;$$

and then for $k = 2, \cdots, 9$, solve $\mathbf{P}_k \mathbf{R}_{k-1} = \mathbf{E}_k$ for $\mathbf{P}_k$, and

$$\mathbf{R}_k = \mathbf{D}_k - \mathbf{P}_k \mathbf{F}_{k-1}.$$

For the boundary components,

$$\mathbf{Q}_1 \mathbf{R}_1 = \mathbf{G}_1$$

$$\mathbf{Q}_k \mathbf{R}_k = \mathbf{G}_k - \mathbf{Q}_{k-1} \mathbf{F}_{k-1}, \quad k = 2, \cdots 9,$$

$$\mathbf{S}_1 = \mathbf{H}_1$$

$$\mathbf{S}_k = \mathbf{H}_k - \mathbf{P}_k \mathbf{S}_{k-1}, \quad k = 2, \cdots 9$$

$$\mathbf{R}_{10} = \mathbf{D}_{10} - \sum_{k=1}^{9} \mathbf{Q}_k \mathbf{S}_k.$$

The new matrix equation

$$\mathbf{L}_m \mathbf{U}_m \mathbf{X}_m = \mathbf{B}_m, \quad m = 1, 2, \cdots 15 \qquad \text{(A10)}$$

is solved in the usual way in two steps:

$$\mathbf{L}_m \mathbf{Y}_m = \mathbf{B}_m, \quad m = 1, 2, \cdots 15, \qquad \text{(A11)}$$

and then

$$\mathbf{U}_m \mathbf{X}_m = \mathbf{Y}_m, \quad m = 1, 2, \cdots 15. \qquad \text{(A12)}$$

These two equations are easy to solve because of the simplicity of the coefficient matrices. Whenever equations involving the submatrices must be solved, we again use **L–U** decomposition.

For different forcing function $\mathbf{B}_m$, such as diabatic heating, transient vorticity flux convergence, orography etc., with the same zonal mean basic state, this method is very efficient because one only has to compute the matrix elements in $\mathbf{L}_m$ and $\mathbf{U}_m$ once. The time required to solve Eqs. (A11)–(A12) when $\mathbf{U}_m$ and $\mathbf{L}_m$ are known is negligible compared to the time required to perform the block tridiagonal decomposition.

b. *Linear model with asymmetric basic state*

The steady GCM equations can be linearized about a zonally asymmetric basic state as well. In this case, one has to add terms that involve longitudinal derivatives of the basic state variables in Eqs. (A1)–(A6). These terms are

$$-\frac{RT'}{a}\frac{\partial \overline{\ln P_*}}{\partial \lambda}: \quad \text{in B' of (A1) and (A2)},$$

$$\frac{\kappa \bar{T}}{\cos\theta}\frac{U'}{a\cos\theta}\frac{\partial \overline{\ln P_*}}{\partial \lambda} + \frac{\kappa T'}{\cos\theta}\frac{\bar{U}}{a\cos\theta}\frac{\partial \overline{\ln P_*}}{\partial \lambda}: \quad \text{in (A3)},$$

$$\frac{U'}{a\cos^2\theta}\frac{\partial \overline{\ln P_*}}{\partial \lambda}: \quad \text{in (A5)},$$

and

$$-\frac{\tilde{U}'}{a\cos^2\theta}\frac{\partial \overline{\ln P_*}}{\partial \lambda}: \quad \text{in (A6)}. \qquad \text{(A13)}$$

The same spectral expansion and vertical finite difference are used for this case, but now the spectral components are coupled in zonal wavenumber space. We continue to think of the zonal mean of all fields as given, and solve only for the deviations from zonal symmetry. For R15 spectral truncation, there are 30 real degrees of freedom in zonal direction. The coefficient matrix **A** is now a real matrix of rank $(5 \times 9 + 1) \times 30 \times 16 = 22080$. Even consider the vertical decoupling, one still deals with at least 25 $(30 \times 16 \times 5) = 2400 \times 2400$ submatrices. Given the size of these matrices, we decided to retain only five zonal wavenumbers, which reduces the submatrix size to 800×800. The solution is otherwise exactly the same as for the symmetric case.

c. *Steady nonlinear model*

We use a simple iteration procedure to obtain steady nonlinear solutions that has been successfully implemented by P. Valdes (personal communication, 1989) in a similar model. The intention is to minimize the number of times that one must perform the very time-consuming block **L–U** decomposition for a linear problem about a zonally asymmetric basic state. To obtain one of the nonlinear solutions for the weak anomaly experiment, no more than four such decompositions were required using the method.

Let $\mathbf{N}(\mathbf{X}) = \mathbf{AX} + \mathbf{X}^2 = \mathbf{F}$ represent the nonlinear problem to be solved. Start by linearizing about the given zonally symmetric flow, $\mathbf{AX} = \mathbf{F}$, and for small forcing amplitude, iterate until convergence to a nonlinear solution is obtained:

$$\mathbf{X}_1 = \mathbf{A}^{-1}\mathbf{F};$$

$$\mathbf{X}_n = \mathbf{A}^{-1}(\mathbf{F} - \mathbf{X}_{n-1}^2). \qquad \text{(A14)}$$

Increase the strength of the forcing slowly, using as a first guess the solution just obtained for weaker forcing, until this procedure no longer converges. At this point, linearize **N** about the last asymmetric nonlinear solution obtained, and repeat this procedure, replacing **A** by this new linear operator **A'**. Continue increasing the strength of the forcing until the solution diverges. Update the linear operator once again with the last nonlinear solution obtained and repeat. The **L–U** decomposition need only be performed when the matrix **A'** is updated. A large number of iterations can be used in each step to insure accurate convergence, and small increments in forcing amplitude can also be used, without increasing the cost of the computation sub-

stantially. For the calculations in section 4, we typically use no more than 15 iterations for each amplitude step and take 20 steps in amplitude before reaching the required forcing.

REFERENCES

Blackmon, M. L., G. W. Branstator, G. T. Bates and J. E. Geisler, 1987: An analysis of equatotial Pacific sea surface temperature anomaly experiments in general circulation models with and without mountains. *J. Atmos. Sci.*, **44**, 1828–1844.

Branstator, G. W., 1985: Analysis of general circulation model sea-surface temperature anomaly simulations using a linear model. Part I: Forced solutions. *J. Atmos. Sci.*, **42**, 2225–2241.

Cook, K. H., and I. M. Held, 1988: Stationary waves of the ice age climate. *J. Climate*, **1**, 807–819.

Edmon, H. J., B. J. Hoskins and M. E. McIntyre, 1980: Eliassen–Palm cross-sections for the troposphere. *J. Atmos. Sci.*, **37**, 2600–2616.

Geisler, J. E., M. L. Blackmon, G. T. Bates and S. Munoz, 1985: Sensitivity of January climate response to the magnitude and position of equatorial Pacific sea surface temperature anomalies. *J. Atmos. Sci.*, **42**, 1037–1049.

Gill, A. E., 1980: Some simple solutions for heat induced tropical circulation. *Quart. J. Roy. Meteor. Soc.*, **106**, 447–462.

Gordon, C. T., and W. F. Stern, 1982: A description of the GFDL global spectral model. *Mon. Wea. Rev.*, **110**, 625–644.

Haarsma, R. J., and J. D. Opsteegh, 1989: Nonlinear response to anomalous tropical forcing. *J. Atmos. Sci.*, **46**, 3240–3255.

Held, I. M., and B. J. Hoskins, 1985: Large-scale eddies and general circulation of the troposphere. *Advances in Geophysics*, Vol. 28, Academic Press, 3–29.

——, and I.-S. Kang, 1987: Barotropic models of the extratropical response to El Niño. *J. Atmos. Sci.*, **44**, 3576–3586.

——, S. W. Lyons and S. Nigam, 1989: Transients and the extratropical response to El Niño. *J. Atmos. Sci.*, **46**, 163–174.

Hendon, H. H., 1986: The time-mean flow and variability in a nonlinear model of the atmosphere with tropical diabatic forcing. *J. Atmos. Sci.*, **43**, 72–88.

Hoskins, B. J., and D. J. Karoly, 1981: The steady linear response of a spherical atmosphere to thermal and orographic forcing. *J. Atmos. Sci.*, **38**, 1179–1196.

——, I. N. James and G. H. White, 1983: The shape, propagation, and mean-flow interaction of large-scale weather systems. *J. Atmos. Sci.*, **40**, 1545–1612.

Kok, C. J., and J. D. Opsteegh, 1985: On the possible cause of anomalies in seasonal mean circulation pattern during the 1982/83 El Niño event. *J. Atmos. Sci.*, **42**, 677–694.

Lau, N.-C., 1985: Modeling the seasonal dependence of the atmospheric response to observed El Niños in 1962–76. *Mon. Wea. Rev.*, **113**, 1970–1996.

Manabe, S., D. G. Hahn and J. L. Holloway, 1979: Climate simulation with GFDL spectral models of the atmosphere. GARP Publ. Ser. No. 22, WMO, Geneva,

Neelin, J. D., 1988: A simple model for surface stress and low-level flow in the tropical atmosphere driven by prescribed heating. *Quart. J. Roy. Meteor. Soc.*, **114**, 747–770.

Nigam, S., I. M. Held and S. W. Lyons, 1986: Linear simulation of the stationary eddies in a general circulation model. Part I: The no-mountian model. *J. Atmos. Sci.*, **43**, 2944–2961.

——, —— and ——, 1988: Linear simulation of the stationary eddies in a general circulation model. Part II: The mountain model. *J. Atmos. Sci.*, **45**, 1433–1452.

Palmer, T. N., and D. A. Mansfield, 1986: A study of wintertime circulation anomalies during past El-Niño events, using a high resolution general circulation model. I: Influence of model climatology. *Quart. J. Roy. Meteor. Soc.*, **112**, 613–638.

Plumb, R. A., 1986: Three-dimensional propagation of quasi-geostrophic eddies and its relationship with the eddy forcing of the time mean flow. *J. Atmos. Sci.*, **43**, 1651–1678.

Sardeshmukh, P. D., and B. J. Hoskins, 1985: Vorticity balances in the tropics during the 1982–83 El Niño-Southern Oscillation event. *Quart. J. Roy. Meteor. Soc.*, **111**, 261–278.

Schneider, E. K., 1989: A method for direct solution of a steady linearized spectral general circulation model. *Mon. Wea. Rev.*, **117**, 2137–2141.

Simmons, A. J., 1982: The forcing of stationary wave motion by tropical diabatic heating. *Quart. J. Roy. Meteor. Soc.*, **108**, 503–534.

——, J. M. Wallace and G. W. Branstator, 1983: Barotropic wave propagation and instability and atmospheric teleconnection patterns. *J. Atmos. Sci.*, **40**, 1363–1392.

Trenberth, K. E., G. W. Branstator and P. A. Arkins, 1988: Origins of the 1988 North American drought. *Science*, **242**, 1640–1645.

Wallace, J. M., and N.-C. Lau, 1985: On the role of barotropic energy conversions in the general circulation. *Advances in Geophysics*, Vol. 28, Academic Press, 33–72.